Transformations of neural representations in a social behaviour network

https://doi.org/10.1038/s41586-022-05057-6

Received: 26 March 2021

Accepted: 29 June 2022

Published online: 3 August 2022

Check for updates

Bin Yang[1,2], Tomomi Karigo[1,2,3] & David J. Anderson[1,2]✉

Mating and aggression are innate social behaviours that are controlled by subcortical circuits in the extended amygdala and hypothalamus[1–4]. The bed nucleus of the stria terminalis (BNSTpr) is a node that receives input encoding sex-specific olfactory cues from the medial amygdala[5,6], and which in turn projects to hypothalamic nuclei that control mating[7–9] (medial preoptic area (MPOA)) and aggression[9–14] (ventromedial hypothalamus, ventrolateral subdivision (VMHvl)), respectively[15]. Previous studies have demonstrated that male aromatase-positive BNSTpr neurons are required for mounting and attack, and may identify conspecific sex according to their overall level of activity[16]. However, neural representations in BNSTpr, their function and their transformations in the hypothalamus have not been characterized. Here we performed calcium imaging[17,18] of male BNSTpr^{Esr1} neurons during social behaviours. We identify distinct populations of female- versus male-tuned neurons in BNSTpr, with the former outnumbering the latter by around two to one, similar to the medial amygdala and MPOA but opposite to VMHvl, in which male-tuned neurons predominate[6,9,19]. Chemogenetic silencing of BNSTpr^{Esr1} neurons while imaging MPOA^{Esr1} or VMHvl^{Esr1} neurons in behaving animals showed, unexpectedly, that the male-dominant sex-tuning bias in VMHvl was inverted to female-dominant whereas a switch from sniff- to mount-selective neurons during mating was attenuated in MPOA. Our data also indicate that BNSTpr^{Esr1} neurons are not essential for conspecific sex identification. Rather, they control the transition from appetitive to consummatory phases of male social behaviours by shaping sex- and behaviour-specific neural representations in the hypothalamus.

We first examined the behavioural effects of silencing Esr1^{+} neurons in the principal subdivision of the bed nucleus of the stria terminalis (BNSTpr^{Esr1} neurons) in socially experienced males. Chemogenetic silencing[20] significantly reduced mounting and increased sniffing towards females, and reduced attack towards males, consistent with previous observations in inexperienced males[16] (Extended Data Fig. 1a–m). Next, we optogenetically silenced[21,22] BNSTpr^{Esr1} neurons during either the appetitive or consummatory phase of social interactions with males or females (Fig. 1). Silencing of BNSTpr^{Esr1} cells during approaching or sniffing of males strongly inhibited the transition to, and duration of, attack, but did not significantly alter sniffing itself (Fig. 1e–g and Extended Data Fig. 1n–q). Silencing of BNSTpr^{Esr1} neurons during approaching or sniffing of females significantly reduced both the transition to (around twofold) and duration of (around 2.5-fold) mounting (Fig. 1j–l and Extended Data Fig. 1t), and extended the total time spent sniffing (Extended Data Fig. 1r,s). Interestingly, whereas optogenetic silencing during attack interrupted this behaviour (Fig. 1h,i), silencing during ongoing mounting had no effect (Fig. 1m,n). Optogenetic silencing of BNSTpr^{Esr1} terminals[23–25] in the medial preoptic area (MPOA) or ventromedial hypothalamus, ventrolateral subdivision (VMHvl) showed that the sniff-to-mount transition towards females is primarily dependent on activity in the BNSTpr → MPOA projection (Extended Data Fig. 2l), whereas activity in the BNSTpr → VMHvl projection is necessary for attack (Extended Data Fig. 2i). These data confirm that BNSTpr^{Esr1} activity is required to gate the transition from appetitive to consummatory male social behaviours towards both sexes[16,26], and show that this gating occurs via its projections to MPOA and VMHvl, respectively. They additionally demonstrate a requirement for BNSTpr^{Esr1} activity during ongoing attack (but not mounting)[27].

A previous study concluded that BNSTpr^{AB} neurons are required for intruder sex recognition, based on male versus female cue-preference tests[16]. Males emit ultrasonic vocalizations (USVs) in response to female but not male urine[9,28]. We performed bilateral optogenetic silencing of BNSTpr^{Esr1} neurons using GtACR2 and tested both cue preference and USVs. Consistent with earlier data[16], we observed a reduced preference for female over male cues (Extended Data Fig. 1r,w). Surprisingly, however, there was no loss of USVs towards female urine or intact females (Extended Data Fig. 1s,x). Thus, whereas silencing of BNSTpr^{Esr1} neurons reduced males' preference for female cues, it did not eliminate their ability to recognize and distinguish female versus male cues.

[1]Division of Biology and Biological Engineering 140-80, TianQiao and Chrissy Chen Institute for Neuroscience, California Institute of Technology, Pasadena, CA, USA. [2]Howard Hughes Medical Institute, California Institute of Technology, Pasadena, CA, USA. [3]Present address: Kennedy Krieger Institute, Johns Hopkins School of Medicine, Baltimore, MD, USA. ✉e-mail: wuwei@caltech.edu

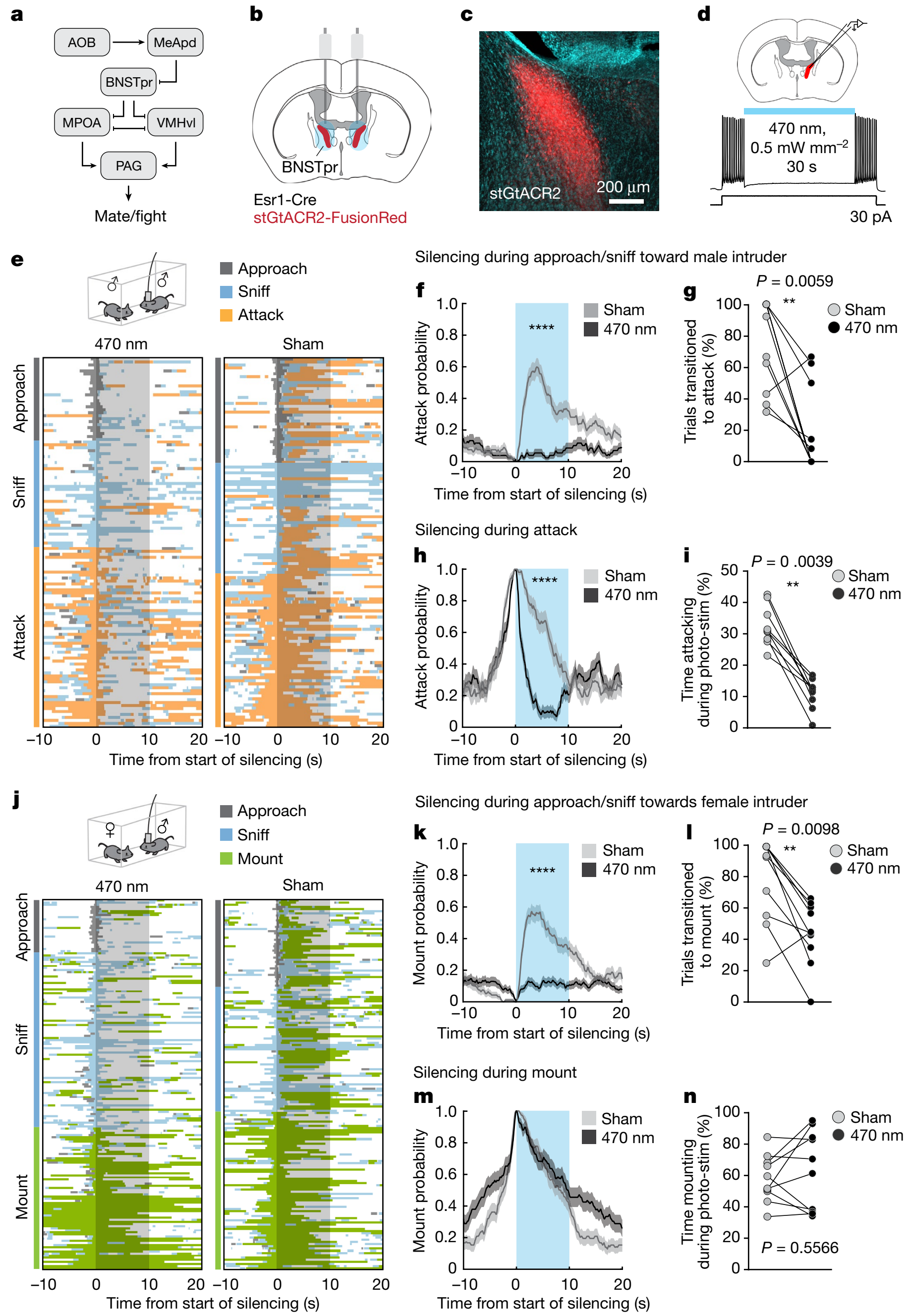

Fig. 1 | BNSTpr^{Esr1} neurons are necessary for the transition from appetitive to consummatory social behaviours in sexually experienced male mice. **a**, Schematic of circuit under study. Bars represent inhibitory connections and arrows represent excitatory connections. AOB, accessory olfactory bulb; PAG, periaqueductal grey. **b**, Illustration of bilateral optogenetic silencing in BNSTpr. **c**, Representative image showing stGtACR2 expression in BNSTpr. Similar expression patterns were observed in all animals tested ($n = 10$). **d**, Whole-cell voltage clamp showing light-mediated silencing of BNSTpr^{Esr1} neurons in an acute slice preparation. **e**–**n**, Techniques used to investigate social behaviours. **e**,**j**, Raster plots showing distribution of social behaviours relative to optogenetic silencing. **f**,**h**,**k**,**m**, Mean probability of behaviour occurring relative to onset of optogenetic silencing. **g**,**l**, Percentage of trials that transitioned to attack (**g**) or mount (**l**). **i**,**n**, Duration of attack (**i**) or mount (**n**) as a percentage of the 10 s optogenetic silencing interval. Statistics: two-sided Wilcoxon signed-rank test (**g**,**i**,**l**,**n**) or two-sided Kolmogorov–Smirnov test (**f**,**h**,**k** **m**). Values are plotted as mean ± s.e.m. $^{****}P < 0.0001$, $^{***}P < 0.001$, $^{**}P < 0.01$, $^{*}P < 0.05$. Male–male trials: $n = 131$ stimulus (stim) and $n = 125$ sham trials pooled from ten mice. Male–female trials: $n = 181$ stim and $n = 170$ sham trials pooled from ten mice. Mouse brain image in **b** reproduced with permission from ref. [41]. Mouse images in **e**,**j** reproduced from ref. [19].

Distinct BNSTpr^{Esr1} subsets encode conspecific sex

Previous bulk calcium measurements of BNSTpr^{AB} neurons suggested that intruder sex is encoded by overall activity, such that strong activity indicates a female whereas weaker activity indicates a male[16]. To show how sex and social behaviours are represented in BNSTpr at the single-cell level, we imaged BNSTpr^{Esr1} neurons (a subset partially overlapping with, but larger than, AB neurons[29]) expressing jGCaMP7f[30] using a micro-endoscope (Inscopix, Inc.; Fig. 2a). By use of a prism-coupled gradient refractive index (GRIN) lens, we were able to image the dorsoventral extent of this elongated nucleus in behaving mice, yielding almost threefold more units per session compared with conventional cylindrical GRIN lenses (Fig. 2b,c and Extended Data Fig. 3a–h).

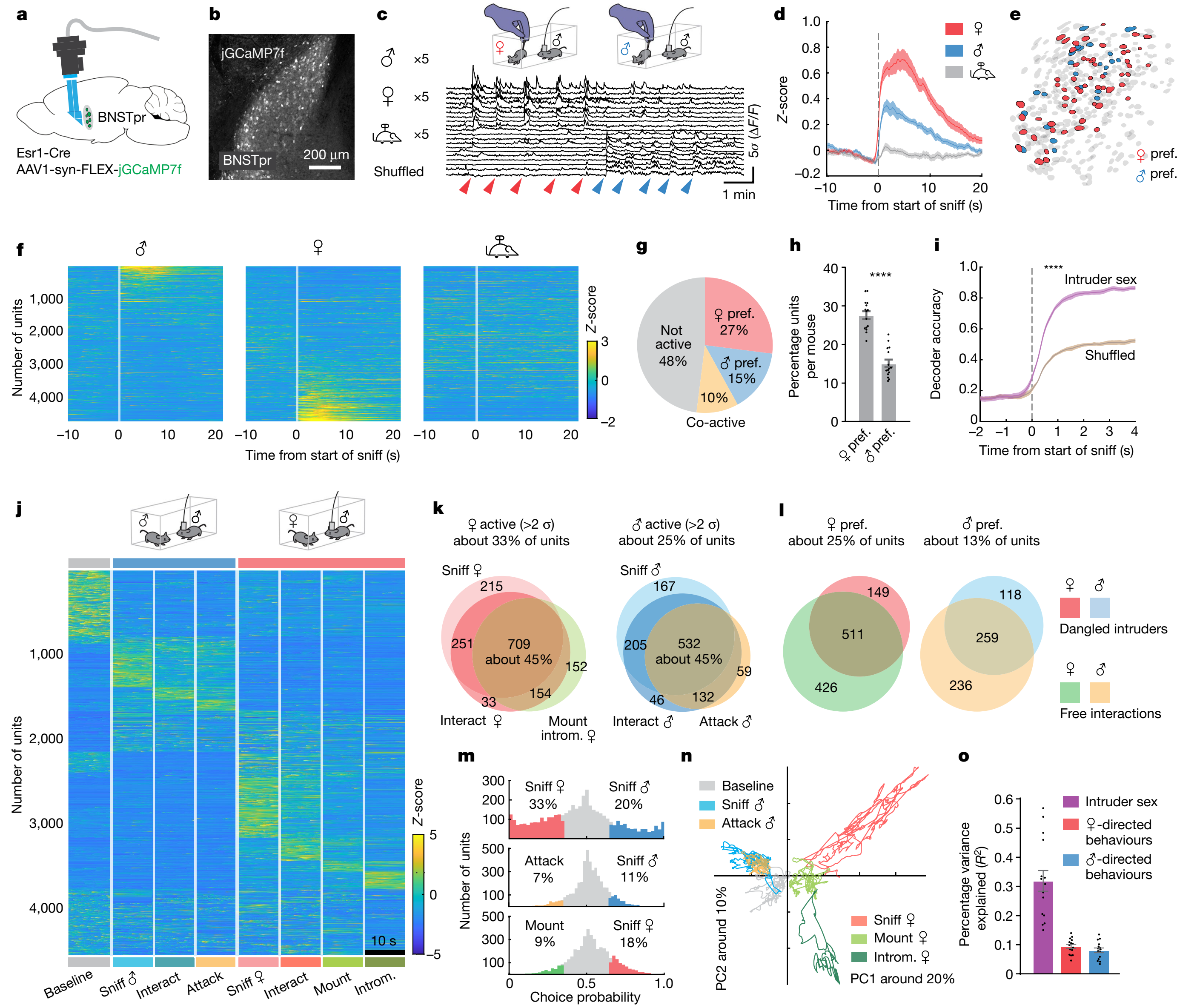

Fig. 2 | BNSTpr^{Esr1} neurons represent intruder sex via a cell-identity code. **a**, Illustration of BNSTpr micro-endocope imaging using a prism-coupled GRIN lens. **b**, Representative image showing jGCaMP7f expression in BNSTpr. Similar expression patterns were observed in 20 mice. **c**, Imaging experiment paradigm and responses of 20 example neurons during dangled presentation of conspecifics. **d**, Mean responses of BNSTpr^{Esr1} neurons during five stimulus presentations. **e**, Spatial map of female- and male-preferring units from one representative mouse. **f**, Single-unit responses during five repeated dangling presentations of male, female or toy mice. **g**, Mean percentages of male- or female-preferring or co-active units (calculated by choice probability; Methods). **h**, Percentage of male- or female-preferring units per imaged animal. **i**, Performance of time-evolving SVM decoders (Methods) of intruder sex. **j**, Raster plot of BNSTpr neuronal activity during male–male or male–female unrestrained social interactions. For comparative purposes, all frames containing each behaviour scored during a 30 min social interaction were concatenated and binned into 10 s intervals; average responses of each unit across all bins are shown. **k**, Venn diagram of units that are >2 σ over pre-intruder baseline during male–male/male–female interactions. Colour coding as in **j**. **l**, Venn diagram of units that are male- or female-preferring (determined by choice probability) during dangled presentations of, or free interactions with, intruders. **m**, Choice probability histograms and percentages of tuned units. **n**, Population activity vectors in the first two PCs space during male- and female-directed behaviours, from one example mouse. **o**, Variance (R^2) in population activity that can be explained by either conspecific sex or male- or female-directed consummatory behaviour. Statistics: two-sided Wilcoxon signed-rank test (**h**); two-sided Kolmogorov–Smirnov test (**i**). Values are plotted as mean ± s.e.m. $^{****}P < 0.0001$, $n = 15$ mice. Mouse brain image in **a** reproduced with permission from ref. [41]. Mouse images in **c**,**j** reproduced from ref. [19].

We first performed trials in which male, female or toy mice suspended by their tails were presented to male residents in their home cage (five trials each, 10 s per trial), permitting sniffing but not mounting or attack[19]. We observed distinct BNSTpr^{Esr1} populations responding to either male or female 'dangled' intruders, but not to toy mice (Fig. 2c,f and Extended Data Fig. 4a). The average downsampled bulk calcium peak response (five 10 s trials) to female intruders was around twofold that of male intruders (Fig. 2d), explaining previous bulk calcium imaging results[16]. Analysis of single-unit calcium responses (extracted using CNMF-E[31,32]; Methods) to intruders showed that 27% of the units were female preferring (determined by choice probability[19] (CP; Methods)) versus 15% that were male preferring (Fig. 2g,h and Extended Data Fig. 4e). Qualitatively similar results were obtained by imaging of BNSTpr^{AB} neurons[16], a functionally equivalent subset of BNSTpr^{Esr1}

neurons[26] (Extended Data Fig. 4j–l). A temporal linear decoder[9] (support vector machine (SVM)) trained on BNSTpr^{Esr1} data could identify the sex of a dangled intruder, in held-out test data, within 1 s of intruder presentation ($P < 0.0001$) compared with shuffled control data (Fig. 2i), suggesting that olfactory cues are sufficient to generate distinct cellular representations of intruder sex in BNSTpr. Male- and female-preferring cells were not topographically segregated but appeared intermingled (Fig. 2e).

We asked next whether BNSTpr^{Esr1} population activity also represents distinct social behaviours, by imaging under conditions in which the resident male freely interacted with male or female intruders (4,585 units from 15 mice). We constructed raster plots of population activity during a 10 s interval from each of eight different conditions (baseline, sniff male/female, interact with male/female, attack, mount and intromission (introm.); Methods and Fig. 2j). Overall, ~33% of imaged units were active (>2 σ) during female encounters whereas ~25% were activated during male encounters. Of these, roughly 45% were activated during appetitive and/or consummatory behaviours towards the intruder (Fig. 2k, orange circle and Extended Data Fig. 4b–d). Approximately 77% of the female-preferring (511 out of 660) and 70% of the male-preferring (259 out of 377) units that exhibited a sex preference during dangling trials retained this preference during subsequent unrestrained social interactions (Fig. 2l).

We computed the tuning of BNSTpr^{Esr1} neurons for intruder sex or specific behaviours using choice probability[19], a binary comparison. Among all units that were active during appetitive and/or consummatory behaviours, a larger percentage were male or female tuned (20% male, 33% female) than were consummatory behaviour tuned (7% attack, 9% mount) (Fig. 2m and Extended Data Fig. 4f). Principle component (PC) analysis indicated that the largest source of variance in neural activity was explained by intruder sex (Fig. 2n, PC1). Linear regression (Methods) showed that intruder sex accounted for >30% of the observed variance whereas only 9 and 8% of variance was explained by behaviour towards females and males, respectively (Fig. 2o and Extended Data Fig. 3i). Together, these results suggest that a major source of variance in BNSTpr^{Esr1} population activity is the sex of the intruder (or an internal motive state highly correlated with intruder sex) and that sex is represented by population coding, as in MPOA and VMHvl (refs. [9,19]).

BNSTpr^{Esr1} neurons control hypothalamic sex coding

We next directly compared representations of intruder sex in medial amygdala (MeApd), BNSTpr, VMHvl and MPOA Esr1$^+$ neurons imaged under identical conditions (Fig. 3a–f and Extended Data Fig. 3i). Like BNSTpr, both MPOA and VMHvl Esr1$^+$ populations contained distinct subsets of male- and female-preferring cells[9,19]. However, whereas among MPOA^{Esr1} and MeApd^{Esr1} neurons female-preferring outnumbered male-preferring units, by about two to one (as in BNSTpr^{Esr1}), among VMHvl^{Esr1} neurons the ratio was reversed (one to two; Fig. 3o,p, grey bars; Extended Data Figs. 3i and 5p–s), consistent with earlier results[6,9,19].

Because BNSTpr projects directly to MPOA and VMHvl (ref. [33]) and encodes conspecific sex identity[16], we hypothesized that inhibition of BNSTpr^{Esr1} neurons should eliminate sex-specific representations in MPOA and VMHvl. To test this, we combined chemogenetic silencing of BNSTpr^{Esr1} neurons using hM4Di[20] with micro-endoscopic imaging of VMHvl^{Esr1} or MPOA^{Esr1} neurons expressing jGCaMP7f[30] (Fig. 3b,c and Extended Data Fig. 5a–o), a method we call ChemoScope. Imaging during presentation of dangled intruders was performed both in control (pre-clozapine-*N*-oxide (CNO)—that is, saline-injected) and experimental (CNO-injected) conditions in the same animals, to permit within-subject comparisons at the single-cell level.

Surprisingly, silencing of BNSTpr^{Esr1} neurons during presentation of dangled male or female intruders did not eliminate sex-specific representations in VMH and MPOA (Fig. 3e versus 3h; 3f versus 3i). A small, but statistically significant, decrease in the separation of male versus female representations was observed in VMHvl, as indicated by Pearson's correlation coefficient and Mahalanobis distance ratio[19] (Fig. 3j,k, VMHvl, opposite sex, grey versus maroon bars). However, the performance of linear decoders of intruder sex, trained on data from MPOA^{Esr1} or VMHvl^{Esr1} neurons, was only slightly decreased in MPOA by silencing of BNSTpr^{Esr1} neurons and was still well above chance (computed using shuffled data). Sex decoding in VMHvl was unaffected (Fig. 3l–m). There was a slight increase in the difference between average *z*-scored responses to females versus males in MPOA, and a larger increase in VMHvl (Fig. 3n), probably reflecting a decrease in the mean response to male intruders in both nuclei, and an increase in the mean response to female intruders in VMHvl (Extended Data Fig. 6q–s).

In contrast to these relatively subtle effects, silencing of BNSTpr^{Esr1} neurons unexpectedly inverted the 2:1 ratio of male- to female-tuned units in VMHvl to the female-dominant ratio seen in MPOA (about 2:1; Fig. 3p, VMH, grey versus maroon bars). This reversal of sex bias in VMHvl reflected both a decrease in male-preferring units and an increase in female-preferring units (Fig. 3o). In MPOA, by contrast, the ratio of female- to male-preferring units was slightly increased by BNSTpr silencing (Fig. 3p,q and Extended Data Fig. 6s,t). Together, these data indicate that the activity of BNSTpr^{Esr1} neurons is not required for the neural coding of intruder sex identity by MPOA^{Esr1} and VMHvl^{Esr1} neurons. Rather, it is required to invert, in VMHvl, the female bias in population representations of intruder sex seen in BNSTpr, MPOA and MeApd[6] to a male bias.

The inversion of sex-tuning bias in VMHvl caused by silencing of BNSTpr^{Esr1} neurons could be explained by one of two mechanisms: (1) conversion, in which a subset of initially male-tuned VMHvl^{Esr1} neurons switched to female-tuning; or (2) selection, in which new female-tuned units appeared and replaced silenced male-tuned units. To distinguish these possibilities, we registered the spatial maps imaged during pre-CNO (saline-injected) and CNO sessions within the same animals and tracked single-unit responses[19] (>60% of all recorded MPOA^{Esr1} units and >55% of all recorded VMHvl^{Esr1} units) during male and female dangling trials, before and after CNO treatment (Fig. 4a,i). Consistent with the data from all (that is, non-tracked) units (Fig. 3p), we observed an approximate inversion of the ratio of male- to female-preferring VMHvl^{Esr1} neurons, from 2.0:1.0 before to 1.0:1.7 after BNSTpr silencing (Fig. 4b,c). By contrast, the ratio of female- to male-preferring MPOA^{Esr1} tracked units was slightly increased in CNO, from 1.5:1.0 to 2.0:1.0 (Fig. 4j,k; compare with Fig. 3p).

Single-unit tracking showed the source of the additional female-preferring Esr1$^+$ units in VMHvl following BNSTpr silencing (Fig. 4h). Almost one-quarter of the female-preferring units (24%) in CNO-treated animals derived from pre-CNO male-preferring units switched sex preference (Fig. 4h, blue; Extended Data Fig. 7q,s, VMH, red bar). Twenty per cent of the female-preferring units after CNO derived from pre-CNO co-active units (that is, responsive to both sexes) that lost male preference (Fig. 4h, yellow; Extended Data Fig. 7l–n), or from initially non-active units that gained female preference (20%) (Fig. 4h, grey; Extended Data Fig. 7g–i). Thus, the inversion of the male sex-tuning bias in VMHvl following BNSTpr silencing was due mostly to the conversion of initially male-preferring, or dual-responsive, units to female-preferring units (Fig. 4g).

In MPOA, following BNSTpr^{Esr1} silencing a substantial proportion of initially male-preferring, co-active or non-active units converted to female-preferring units (Fig. 4o). However, this conversion was partially offset by the silencing of some initially female-preferring units (Fig. 4o and Extended Data Fig. 7c (right), f,k,n). Consequently, the overall proportion of female-preferring MPOA^{Esr1} units did not change greatly after CNO (Fig. 4j,k,p). In contrast to VMHvl, therefore, whereas BNSTpr^{Esr1} silencing converted initially non-female-selective to female-selective units, in MPOA the slight increase in female-tuned units (Fig. 3n,p) was

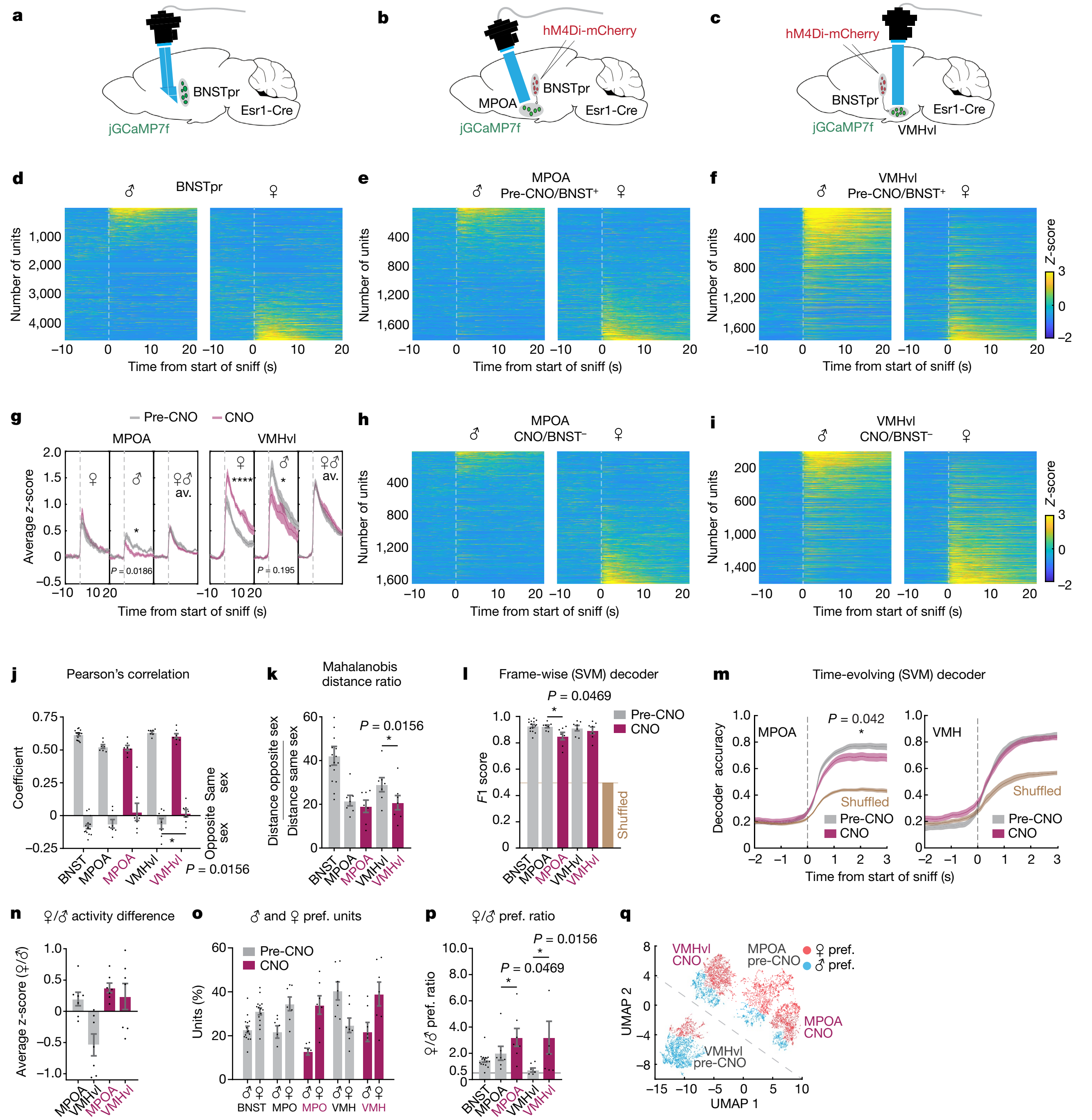

Fig. 3 | BNSTpr is required for male-biased intruder sex representations in VMHvl. **a**, Illustration of BNSTpr micro-endoscope imaging. **b**,**c**, Illustration of ChemoScope imaging in MPOA (**b**) and VMHvl (**c**) while silencing BNSTpr. **d**–**f**,**h**,**i**, Average single-unit responses imaged during five repeated dangling presentations of male or female mice in BNSTpr (**d**), pre-CNO MPOA (**e**) and pre-CNO VMHvl (**f**), or treated with CNO (7.5 mg kg^{-1} CNO i.p.) MPOA (**h**) or VMHvl (**i**). Pre-CNO animals received an equivalent volume of saline i.p. CNO controls shown in Extended Data Fig. 1l, **g**, Average bulk (downsampled) calcium responses to dangled female or male stimuli, or combined male and female responses, before (that is, saline injected) versus after the application of CNO, in MPOA (left) and VMHvl (right). **j**,**k**, Average Pearson's correlation coefficient (**j**) and average Mahalanobis distance ratio (**k**) between population responses to dangled mice of the same or opposite sex in BNSTpr, MPOA and VMHvl, ±CNO. **l**,**m**, Performance of frame-wise (**l**) and time-evolving (**m**) decoders. **n**, Average difference between responses to female or male stimuli in MPOA and VMHvl. **o**, Average percentage of male- versus female-preferring units. **p**, Ratio of female-to male-preferring units. **q**, Supervised UMAP embedding of population responses to male and female stimuli across MPOA and VMHvl (Methods). Statistics, two-sided Kolmogorov–Smirnov test (**g**,**m**) or two-sided Wilcoxon signed-rank test (**j**–**l**, **p**). Values are plotted as mean ± s.e.m. $^{****}P < 0.0001$, $^{***}P < 0.001$, $^{**}P < 0.01$, $^{*}P < 0.05$; $n = 7$ mice per imaged region. Mouse brain images in **a**–**c** reproduced with permission from ref. [41].

primarily due to a substitution of new female-tuned units for others that became inactive. There was no significant change in the percentage of tracked male- or female-tuned units in either MPOA or VMHvl in animals injected with saline on two consecutive days (Extended Data Fig. 5p–s).

BNSTpr^{Esr1} neurons control social behaviour coding

To investigate how silencing of BNSTpr^{Esr1} neurons would affect hypothalamic activity during mounting and attack, we tracked single-unit

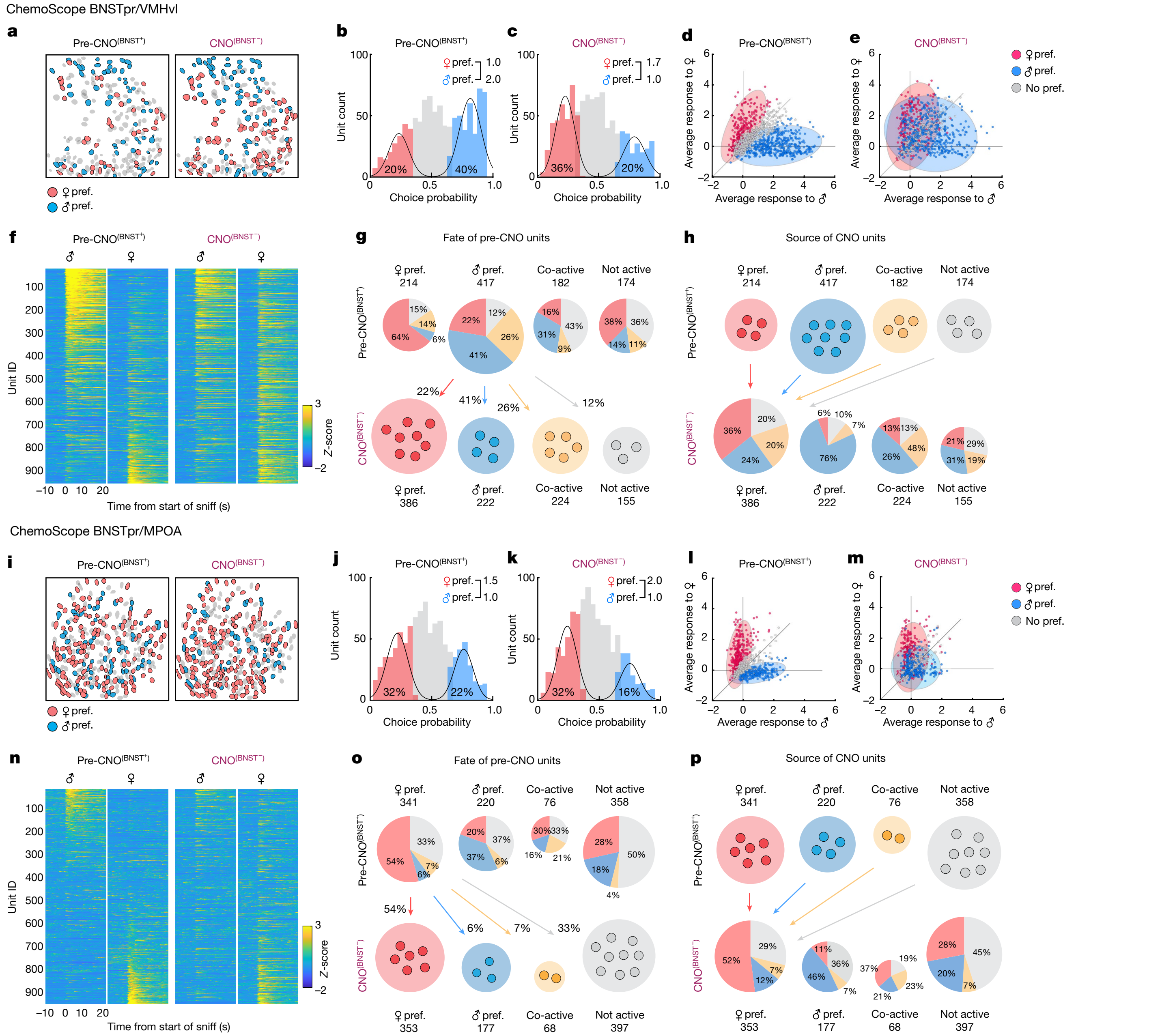

Fig. 4 | Differential effect of BNSTpr silencing on sex representations in VMHvl and MPOA shown by sequential imaging of identified units. **a**–**p**, Sequential imaging of identified units. **a**,**i**, Spatial maps of tracked male- and female-preferring units in VMHvl (**a**) and MPOA (**i**) before and after CNO application. **f**,**n**, Single-unit responses to dangled male or female stimuli in VMHvl (**f**) or MPOA (**n**) before versus after CNO application. Sorting of units is the same for pre- versus post-CNO. **b**,**c**,**j**,**k**, Histograms of male- versus female-tuned units determined by choice probability from single-unit responses to dangled intruders. **d**,**e**,**l**,**m**, Scatter plots of single-unit responses to dangled male and female mice before and after CNO application in VMHvl (**d**,**e**) or MPOA (**l**,**m**). Each dot (**d**,**e**,**l**,**m**) represents a single neuron, with the colour indicating its male/female preference before CNO application. Distribution of male- and female-preferring units before (**d**,**l**) and after CNO (**e**,**m**) is shown as coloured ellipses. **g**,**h**,**o**,**p**, Pie charts showing fates (**g**,**o**) and sources (**h**,**p**) of units in VMHvl (**g**,**h**) and MPOA (**o**,**p**) before versus after CNO treatment, respectively. The percentage of units of each type that retained or switched sex preference, responded to both sexes (co-active) or responded to neither sex (not active) is indicated.

responses in MPOA^{Esr1} or VMHvl^{Esr1} neurons before and after unilateral silencing of BNSTpr in freely behaving animals (Fig. 5a). Because BNSTpr → hypothalamic projections are primarily ipsilateral[33], by performing silencing and imaging on one side of the brain and leaving the other unperturbed this design allowed normal social behaviour even in CNO, due to redundant contralateral circuits. Thus, any observed changes in neural activity on the silenced side cannot be due to a loss of social behaviour, which requires bilateral BNSTpr^{Esr1} silencing (Fig. 1b and Extended Data Fig. 1a).

In MPOA, female-directed sniffing versus mounting was represented by largely distinct groups of neurons (Fig. 5b, pre-CNO). CNO silencing of BNSTpr^{Esr1} significantly decreased the activity of mount-selective cells, with a concomitant increase in sniff-active cells during mounting behaviour (Fig. 5c–f). Thus, during BNSTpr^{Esr1} silencing of cellular responses, female-directed sniffing versus mounting became more similar than in controls (Fig. 5b, CNO). A corresponding decrease in the fraction of variance in neural activity explained by female-directed behaviours was also observed (Fig. 5g).

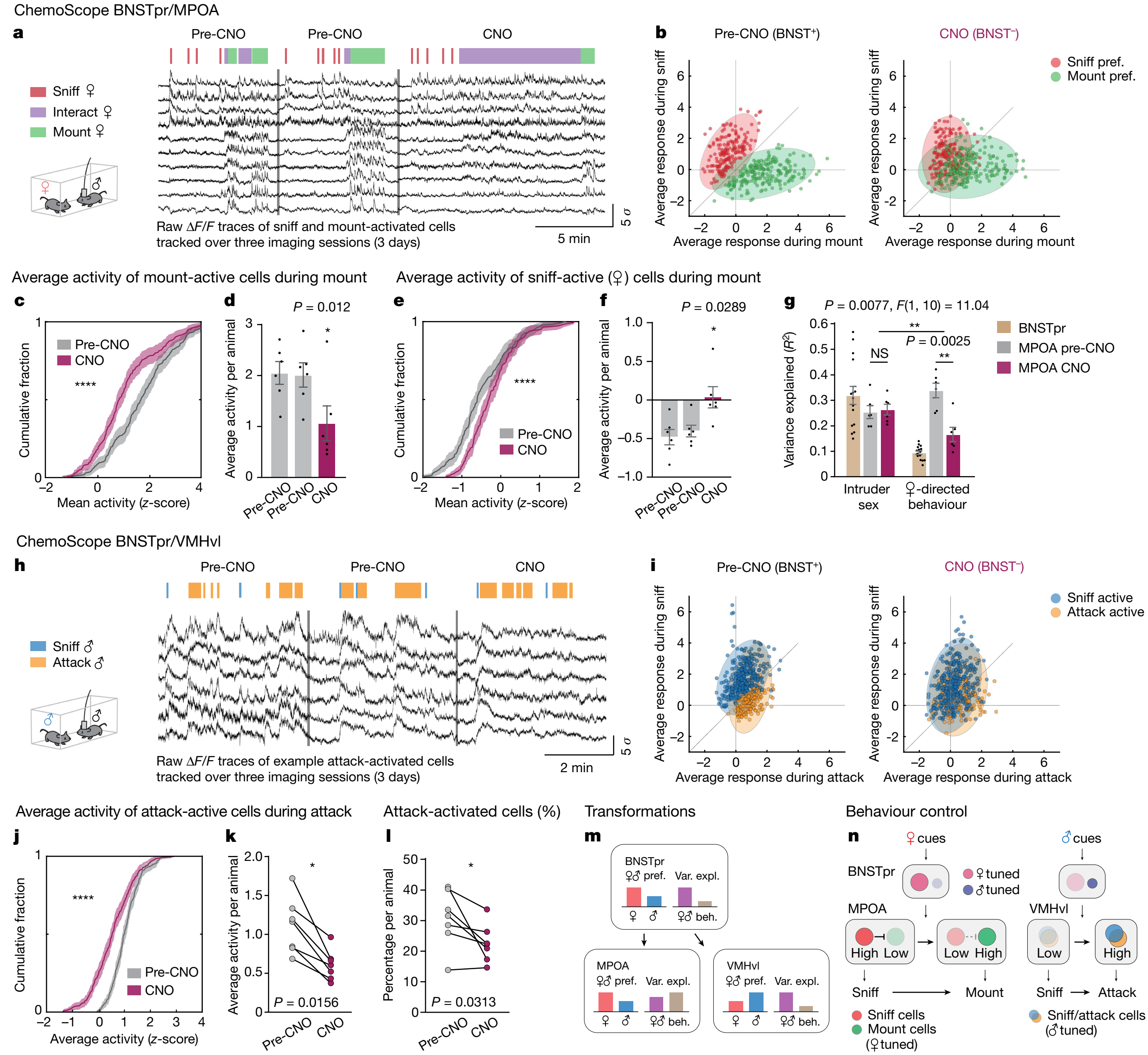

Fig. 5 | Differential effect of BNSTpr silencing on behaviour representations in MPOA and VMHvl shown by unilateral ChemoScope imaging. a–n, Effect of BNSTpr silencing on behaviour representations in MPOA and VMHvl. **a**,**h**, Responses from example neurons tracked over three imaging sessions in MPOA (**a**) and VMHvl (**h**). **b**,**i**, Scatter plot of single-unit responses to sniff and mount females in MPOA (**b**), or to sniff and attack males in VMHvl (**i**). **b**,**i**, Each dot represents a single neuron, with its colour indicating its tuning before CNO application. Distribution of sniff versus mount MPOA units (**b**) and sniff versus attack VMHvl units (**i**) before and after CNO is shown as coloured ellipses. **c**–**f**, Cumulative fractions (**c**,**e**) and bar graphs (**d**,**f**) of MPOA single-unit responses to initially (that is, in saline-injected animals/pre-CNO) mount-activated (**c**) or sniff-active cells (**e**) during mounting. **g**, Variance (R^2) in population activity that can be explained by either intruder sex or female-directed consummatory behaviour. **j**,**k**, Cumulative fractions (**j**) and scatter plots (**k**) of VMHvl single-unit responses to initially attack-active cells during attack. **l**, Percentage of attack-active cells per animal. **m**, Diagram summarizing observed transformations of sex and behaviour representations from BNSTpr to MPOA and VMHvl. pref., fraction of units that are either female- (red bars) or male- (blue bars) preferring neurons; var. expl., fraction of variance explained (R^2) by intruder sex (purple bars) or consummatory behaviour (light brown bars). **n**, Schematic illustrating the role of BNSTpr^{Esr1} neurons in controlling the transition from sniffing to mounting or attack. Pale circles denote low activity, saturated circles high activity. Vertical arrows indicate net functional influences and requirements for BNSTpr activity; horizontal arrows indicate time-dependent transitions. Statistics: two-sided Kolmogorov–Smirnov test (**c**,**e**,**j**), two-sided Wilcoxon signed-rank test (**k**,**l**), Friedman test with Dunn's correction (**d**,**f**) or two-way ANOVA with Bonferroni correction (**g**). $^{****}P < 0.0001$, $^{***}P < 0.001$, $^{**}P < 0.01$, $^{*}P < 0.05$; NS, not significant. Values are plotted as mean ± s.e.m. For ChemoScope BNSTpr/MPOA, $n = 6$ mice (**d**,**f**,**g**); for ChemoScope BNSTpr/VMHvl, $n = 7$ mice (**k**,**l**). Mouse images in **a**,**h** reproduced from ref. [19].

In contrast to MPOA, in VMHvl, male-directed sniffing and attack are represented by largely overlapping neuronal populations (Fig. 5h)[9,19]. Following BNSTpr^{Esr1} silencing, both the average activity of those neurons normally active during attack behaviour, as well as well as the percentage of attack-active neurons, were significantly reduced (Fig. 5j–l). There was also a decrease in the number of male-selective

VMHvl^{Esr1} neurons (Fig. 5i, CNO; Fig. 4b,c). Together these data show that, in MPOA, unilateral BNSTpr^{Esr1} silencing extended the activity of normally sniff-selective cells into the mounting phase and decreased the activity of mount-selective cells during mounting. In VMHvl it reduced the activity of both mixed-selectivity and attack-selective cells during the attack, but not the sniff, phase. Thus, silencing of BNSTpr^{Esr1} neurons in freely behaving males during social interactions caused distinct changes in neural representations of consummatory behaviour in VMHvl and MPOA. However the average response to males and females in both nuclei remained unchanged (Fig. 3g, male/female average).

Discussion

BNSTpr lies at the interface between the encoding of sex-specific olfactory cues in the medial amygdala and of motive drive states in the hypothalamus that control the consummatory phases of social behaviours. Previous studies suggested that it represents and is essential for the identification of conspecific sex via an intensity code[16], with its requirement for consummatory behaviours presumably reflecting the former function. The data presented here suggest an alternative view.

First, although we confirm that BNSTpr neural activity contains a representation of conspecific sex identity, our cellular resolution calcium imaging shows that female versus male identity is not encoded by a higher versus lower level of activity in this structure, respectively, as suggested by previous bulk calcium measurements[16], but rather by a cell-identity code: distinct subpopulations of BNSTpr^{Esr1} neurons are tuned to males versus females. Because female-tuned neurons outnumber male-tuned cells by around two to one, a higher level of BNSTpr activity is observed in response to females than males when bulk calcium signals are measured by fibre photometry[16]. This approximate two-to-one female-tuning bias is similar to that in MeApd[6] and MPOA[9], but is inverted in VMHvl (ref. [19]). Thus, at each node in the processing pathway, from MeApd →BNSTpr → MPOA/VMHvl, intruder sex is represented as a cell-identity code (Extended Data Fig. 3i).

Second, although BNSTpr^{Esr1} neuronal activity represents intruder sex identity, this activity is not required for identification of conspecific sex[15]. Although we confirmed that BNSTpr^{Esr1} neuronal activity is required for males to show a preference for female cues[16], we find surprisingly that it is not required for them to identify and distinguish females versus males: emission of USVs is observed only in response to female and not male cues, as in control males[8,9]. Consistent with this, intruder sex can be decoded equally well from MPOA^{Esr1} or VMHvl^{Esr1} neural activity in the presence or absence of BNSTpr^{Esr1} activity. Whereas the ability to identify and distinguish females versus males is clearly a prerequisite for a male to show a preference for females, it does not follow that all deficits in female preference necessarily reflect deficient sex identification. Our results call into question the widespread use of male versus female preference assays as a surrogate measure of conspecific sex identification.

Interestingly, female-biased conspecific sex-tuned neural representations have also been observed in the prefrontal cortex, in which they play a role in sex preference behaviour[34]. The causal relationship between conspecific sex tuning in cortical versus subcortical regions remains to be determined. Our results also raise the question of whether the weak male-biased sex tuning observed in MeApd[6] in female mice extends to the structures we have investigated here. Previous bulk calcium imaging studies suggest that BNSTpr AB neurons do not encode intruder sex in females[15], but single-cell analysis was not performed.

Third, whereas it may be intuitive to think that MeApd, BNSTpr and the hypothalamus each play distinct functional roles in the transformation of sex-specific social cues into behaviour, such as social cue representation, sex identification and action selection, respectively, our data on the transformations in neural representations that occur as information flows through this circuit do not support such a strict hierarchical view. Instead, we find that the relative variance explained by intruder sex identity versus behaviour is different in each of these regions. In MPOA, the variance explained by behaviour is higher than that in BNSTpr (and in MeApd) (Fig. 5g,m and Extended Data Fig. 3i), consistent with a gradual shift in the relative representations of sex identity versus behaviour from the amygdala to the hypothalamus. By contrast, the variance explained by intruder sex in VMHvl is higher than that in BNSTpr, largely because the former has very few neurons tuned to specific phases of social behaviour[19]. Rather, the main transformation that occurs from MeApd and BNSTpr to VMHvl is an inversion of the ratio of sex-tuned neurons, from female-dominant to male-dominant, respectively (Fig. 5m).

Surprisingly, when BNSTpr^{Esr1} neurons were silenced chemogenetically, the male sex-tuning bias in VMHvl flipped to a female-tuning bias. Apparently, female-tuning-dominant Esr1^{+} GABAergic neurons in BNSTpr are required to suppress female-specific tuning among VMHvl^{Esr1} glutamatergic neurons. Consistent with this, retrograde imaging indicated that female-biased tuning is present among BNSTpr^{Esr1} neurons that project to VMHvl (as well as to MPOA; Extended Data Fig. 9). Essentially, BNSTpr^{Esr1} neurons are required to maintain a locus where male-tuned neurons predominate within a network that is otherwise dominated by female-tuned neurons. The mechanism whereby the female-biased sex representation in BNSTpr is transformed into a male-biased representation in VMHvl remains to be established, and may involve differential male- or female-biased inputs from other regions such as the posterior amygdala[35–37]. By contrast, silencing of BNSTpr did not significantly alter the female-dominant sex bias in MPOA (if anything, it was slightly increased); rather it reduced the variance explained by behaviour (Fig. 5g). Together, these data indicate a requirement for BNSTpr^{Esr1} neuronal activity in shaping the representations of social behaviour and conspecific sex in MPOA and VMHvl, respectively, albeit to different extents (Fig. 5m).

Finally, our results indicate that the inhibition of mounting and attack behaviour that occurs following BNSTpr^{Esr1} silencing is not secondary to a deficiency in sex identification[16]. Rather, the failure to transition from appetitive to consummatory social behaviour following silencing reflects changes in the pattern of sex- and behaviour-specific tuning among VMHvl^{Esr1} and MPOA^{Esr1} neurons, with no loss of sex identity coding. In what follows, we suggest plausible explanations for how these circuit-level 'mutant phenotypes' may lead to the observed behavioural phenotypes. However, this causality is not directly demonstrated and more complex explanations are certainly possible.

In MPOA, many Esr1^{+} neurons are tuned for specific behaviours, including sniffing or mounting (Fig. 5a and Extended Data Fig. 3i). Accordingly, as males transition from sniffing to mounting, sniff-selective neurons become less active whereas mount-selective neurons become more active. When BNSTpr^{Esr1} neurons are silenced, this change in MPOA neural representations of social behaviour is muted: sniff-selective neurons continue to be active (on the silenced side) as the animal transitions to mounting whereas mount-selective neurons exhibit reduced activity (Fig. 5a–e). Because about 95% of MPOA neurons are GABAergic[26,38], these observations suggest that, in normal animals during sniffing, sniff-selective neurons (or another MPOA subpopulation) may inhibit mount-selective neurons. To transition to mounting, input from BNSTpr^{Esr1} GABAergic neurons may be required to inhibit the sniff-selective population, thereby disinhibiting mount-selective cells (Fig. 5n). In the absence of BNSTpr^{Esr1} activity, mount-selective cells remain inhibited and so this transition is blocked; instead the male continues to sniff the female (Extended Data Fig. 1b, lower).

In VMHvl, sniff- and attack-active cells are largely overlapping (Fig. 5i) but are sex-specific[9,19], with male-tuned neurons outnumbering female-tuned cells by around two to one. During attack, primarily male-tuned neurons are active[9,19]. Optogenetic experiments[9,11,13] and computational modelling[39] suggest that the activity of VMHvl^{Esr1} neurons must reach a certain threshold for males to transition from sniff to attack. In the absence of BNSTpr^{Esr1} activity, female-tuned neurons become dominant in VMHvl and therefore both the number and activity of male-selective neurons are reduced (Fig. 4c and Extended Data Fig. 8a). This reduction may prevent activity in the male-tuned population from reaching the threshold necessary to transition to attack (Fig. 5j–l,n), although increased inhibition from neighbouring GABAergic neurons may also contribute. Together these data suggest that activity in BNSTpr^{Esr1} neurons controls sex and behaviour tuning in MPOA and VMHvl in a manner essential for the transition from sniffing to mounting or attack, respectively.

Functional perturbations and observational studies often yield different views of brain function[40]. Our results demonstrate how calcium imaging can be combined with manipulations of neural activity in freely moving animals to identify and link circuit level to behavioural phenotypes. This combined approach allows an integration of observational and perturbational data to show both the transformations in neural representations that occur as information flows through a circuit, and the potential function of such transformations in the control of behaviour. Future studies should uncover the detailed cellular and synaptic mechanisms that underlie these important transformations.

Online content

Any methods, additional references, Nature Research reporting summaries, source data, extended data, supplementary information, acknowledgements, peer review information; details of author contributions and competing interests; and statements of data and code availability are available at https://doi.org/10.1038/s41586-022-05057-6.

1. Yang, C. F. & Shah, N. M. Representing sex in the brain, one module at a time. *Neuron* **82**, 261–278 (2014).
2. Anderson, D. J. Circuit modules linking internal states and social behaviour in flies and mice. *Nat. Rev. Neurosci.* **17**, 692–704 (2016).
3. Hashikawa, K., Hashikawa, Y., Falkner, A. & Lin, D. The neural circuits of mating and fighting in male mice. *Curr. Opin. Neurobiol.* **38**, 27–37 (2016).
4. Chen, P. & Hong, W. Neural circuit mechanisms of social behavior. *Neuron* **98**, 16–30 (2018).
5. Bergan, J. F., Ben-Shaul, Y. & Dulac, C. Sex-specific processing of social cues in the medial amygdala. *eLife* **3**, e02743 (2014).
6. Li, Y. et al. Neuronal representation of social information in the medial amygdala of awake behaving mice. *Cell* **171**, 1176–1190 (2017).
7. Simerly, R. B. Wired for reproduction: organization and development of sexually dimorphic circuits in the mammalian forebrain. *Annu. Rev. Neurosci.* **25**, 507–536 (2002).
8. Wei, Y.-C. et al. Medial preoptic area in mice is capable of mediating sexually dimorphic behaviors regardless of gender. *Nat. Commun.* **9**, 279 (2018).
9. Karigo, T. et al. Distinct hypothalamic control of same- and opposite-sex mounting behaviour in mice. *Nature* **589**, 258–263 (2020).
10. Ogawa, S. et al. Abolition of male sexual behaviors in mice lacking estrogen receptors α and β (αβERKO). *Proc. Natl Acad. Sci. USA* **97**, 14737 (2000).
11. Lin, D. et al. Functional identification of an aggression locus in the mouse hypothalamus. *Nature* **470**, 221–226 (2011).
12. Yang, T. et al. Social control of hypothalamus-mediated male aggression. *Neuron* **95**, 955–970 (2017).
13. Lee, H. et al. Scalable control of mounting and attack by Esr1^{+} neurons in the ventromedial hypothalamus. *Nature* **509**, 627–632 (2014).
14. Yang, C. F. et al. Sexually dimorphic neurons in the ventromedial hypothalamus govern mating in both sexes and aggression in males. *Cell* **153**, 896–909 (2013).
15. Wei, D., Talwar, V. & Lin, D. Neural circuits of social behaviors: innate yet flexible. *Neuron* **109**, 1600–1620 (2021).
16. Bayless, D. W. et al. Limbic neurons shape sex recognition and social behavior in sexually naive males. *Cell* **176**, 1190–1205 (2019).
17. Ghosh, K. K. et al. Miniaturized integration of a fluorescence microscope. *Nat. Methods* **8**, 871–878 (2011).
18. Ziv, Y. et al. Long-term dynamics of CA1 hippocampal place codes. *Nat. Neurosci.* **16**, 264–266 (2013).
19. Remedios, R. et al. Social behaviour shapes hypothalamic neural ensemble representations of conspecific sex. *Nature* **550**, 388–392 (2017).
20. Armbruster, B. N., Li, X., Pausch, M. H., Herlitze, S. & Roth, B. L. Evolving the lock to fit the key to create a family of G protein-coupled receptors potently activated by an inert ligand. *Proc. Natl Acad. Sci. USA* **104**, 5163–5168 (2007).
21. Govorunova, E. G., Sineshchekov, O. A., Janz, R., Liu, X. & Spudich, J. L. Natural light-gated anion channels: a family of microbial rhodopsins for advanced optogenetics. *Science* **349**, 647–650 (2015).
22. Mahn, M. et al. High-efficiency optogenetic silencing with soma-targeted anion-conducting channelrhodopsins. *Nat. Commun.* **9**, 4125 (2018).
23. Gradinaru, V. et al. Molecular and cellular approaches for diversifying and extending optogenetics. *Cell* **141**, 154–165 (2010).
24. Mahn, M., Prigge, M., Ron, S., Levy, R. & Yizhar, O. Biophysical constraints of optogenetic inhibition at presynaptic terminals. *Nat. Neurosci.* **19**, 554–556 (2016).
25. Zhang, C. et al. Optimized photo-stimulation of halorhodopsin for long-term neuronal inhibition. *BMC Biol.* **17**, 95 (2019).
26. Knoedler, J. R. et al. A functional cellular framework for sex and estrous cycle-dependent gene expression and behavior. *Cell* **185**, 654–671 (2022).
27. Padilla, S. L. et al. Agouti-related peptide neural circuits mediate adaptive behaviors in the starved state. *Nat. Neurosci.* **19**, 734–741 (2016).
28. Nyby, J., Wysocki, C. J., Whitney, G. & Dizinno, G. Pheromonal regulation of male mouse ultrasonic courtship (*Mus musculus*). *Anim. Behav.* **25**, 333–341 (1977).
29. Stanić, D. et al. Characterization of aromatase expression in the adult male and female mouse brain. I. Coexistence with oestrogen receptors α and β, and androgen receptors. *PLoS ONE* **9**, e90451 (2014).
30. Dana, H. et al. High-performance calcium sensors for imaging activity in neuronal populations and microcompartments. *Nat. Methods* **16**, 649–657 (2019).
31. Pnevmatikakis, E. A. et al. Simultaneous denoising, deconvolution, and demixing of calcium imaging data. *Neuron* **89**, 285–299 (2016).
32. Zhou, P. et al. Efficient and accurate extraction of in vivo calcium signals from microendoscopic video data. *eLife* **7**, e28728 (2018).
33. Dong, H.-W. & Swanson, L. W. Projections from bed nuclei of the stria terminalis, posterior division: implications for cerebral hemisphere regulation of defensive and reproductive behaviors. *J. Comp. Neurol.* **471**, 396–433 (2004).
34. Kingsbury, L. et al. Cortical representations of conspecific sex shape social behavior. *Neuron* **107**, 941–953 (2020).
35. Stagkourakis, S., Spigolon, G., Liu, G. & Anderson, D. J. Experience-dependent plasticity in an innate social behavior is mediated by hypothalamic LTP. *Proc. Natl Acad. Sci. USA* **117**, 25789–25799 (2020).
36. Yamaguchi, T. et al. Posterior amygdala regulates sexual and aggressive behaviors in male mice. *Nat. Neurosci.* **23**, 1111–1124 (2020).
37. Zha, X. et al. VMHvl-projecting Vglut1^{+} neurons in the posterior amygdala gate territorial aggression. *Cell Rep.* **31**, 107517 (2020).
38. Moffitt, J. R. et al. Molecular, spatial, and functional single-cell profiling of the hypothalamic preoptic region. *Science* **362**, eaau5324 (2018).
39. Nair, A. et al. An approximate line attractor in the hypothalamus that encodes an aggressive internal state. Preprint at *bioRxiv* https://doi.org/10.1101/2022.04.19.488776 (2022).
40. Jazayeri, M. & Afraz, A. Navigating the neural space in search of the neural code. *Neuron* **93**, 1003–1014 (2017).
41. Paxinos, G. & Watson, C. *The Mouse Brain in Stereotaxic Coordinates* (Elsevier, 2001).

Methods

Mice

All experimental procedures involving the use of live mice or their tissues were carried out in accordance with NIH guidelines and were approved by the Institute Animal Care and Use Committee and the Institute Biosafety Committee at the California Institute of Technology (Caltech). All C57BL/6N mice used in this study, including wild-type and transgenic mice, were bred at Caltech. BALB/c male and female mice were used as intruder mice and either bred at Caltech or purchased from Charles River Laboratories. Experimental mice were used at the age of 2–3 months. Intruder mice were used at the age of 2–6 months and were maintained with three to five cage mates to reduce their aggression. *Esr1*$^{Cre/+}$ knock-in mice (Jackson Laboratory, stock no. 017911) were back-crossed into the C57BL/6N background (>N10) and bred at Caltech. Heterozygous *Esr1*$^{Cre/+}$, or double-heterozygous *Aromatase*$^{Cre/+}$ (ref. [17]) *Ai148/+* (ref. [42]) mice were used for cell-specific targeting experiments, and were genotyped by PCR analysis using genomic DNA from tail or ear tissue. All mice were housed in ventilated micro-isolator cages in a temperature-controlled environment (median temperature 23 °C, humidity 60%), under a reversed 11/13-h dark/light cycle, with ad libitum access to food and water. Mouse cages were changed weekly.

Viruses

The following adeno-associated viruses (AAVs), along with the supplier, injection titres (in viral genome copies ml^{-1} (vg ml^{-1}) and injection volumes (in nanolitres), were used in this study.

AAV1-hSyn1-SIO-stGtACR2-FusionRed (Addgene, no. 105677, around 2×10^{12} vg ml^{-1}, 200 nl), AAV5-hSyn-DIO-hM4D(Gi)-mCherry (Addgene, no. 44362, about 2×10^{12} vg ml^{-1}, 200 nl per injection), AAV5-Ef1a-DIO-eNpHR3.0-eYFP (Halo-eYFP; Extended Data Fig. 2) (Addgene, no. 26966, approximately 4×10^{12} vg ml^{-1}, 200 nl per injection), AAV1-syn-FLEX-jGCaMP7f-WPRE (Addgene, no. 104492, roughly 2×10^{12} vg ml^{-1}, 200 nl per injection), AAVdj-syn-FLEX-FlpO (Janelia Vector Core, around 1×10^{13} vg ml^{-1}, 200 nl per injection), AAVretro-syn-fDIO-jGCaMP7f (Janelia Vector Core, about 2×10^{12} vg ml^{-1}, 200 nl per injection), AAVretro-CBH-DIO-nls-mScarlet (Janelia Vector Core, roughly 1×10^{13} vg ml^{-1}, 200 nl per injection) and AAVretro-CBH-DIO-nls-mNeonGreen (Janelia Vector Core, approximately 1×10^{13} vg ml^{-1}, 200 nl per injection).

Stereotaxic coordinates for virus injection and GRIN lens implantation

Stereotaxic injection coordinates were based on the Paxinos and Franklin atlas[41].

Virus injection: BNSTpr, AP: −0.15, ML: ±0.65, DV: −3.75; VMHvl, AP: −1.5, ML: ±0.75, DV: −5.75; MPOA, AP: 1.0, ML: ±0.3, DV: −4.75; MeApd, AP: −1.65, ML: ±2.1, DV: −4.9).

GRIN lens implantation:

BNSTpr: AP: −0.1, ML: −0.7, DV: −4.5 (⌀0.85 × 7 mm GRIN lens with prism; Extended Data Fig. 3). ⌀, diameter of the GRIN lens.

BNSTpr: AP: −0.2, ML: −0.7, DV: −3.65 (⌀0.6 × 7.3 mm GRIN lens).

MeApd: AP: −1.65, ML: −2.0, DV: −4.75 (⌀0.6 × 7.3 mm GRIN lens).

VMHvl: AP: −1.6, ML: −0.75, DV: −5.6 (⌀0.6 × 7.3 mm GRIN lens).

MPOA: AP: +1.0, ML: −1.0, DV: −5.0 (⌀0.6 × 7.3 mm GRIN lens). Implanted at a 10° tilt in AP axis and a 5° tilt in ML axis to avoid damaging BNSTpr and its projections to MPOA (Extended Data Fig. 5a–j).

Surgeries

Surgeries were performed on socially and sexually experienced adult male *Esr1*$^{Cre/+}$ mice aged 2–3 months. Virus injection and implantation were performed as described previously[9,19]. Briefly, animals were anaesthetized with isoflurane (5% for induction and 1.5% for maintenance) and placed on a stereotaxic frame (David Kopf Instruments). Virus was injected into the target area using a pulled-glass capillary (World Precision Instruments) and a pressure injector (Micro4 controller, World Precision Instruments), at a flow rate of 50 nl min^{-1}. The glass capillary was left in place for 5 min following injection before withdrawal. For micro-endoscope experiments, virus injection and lens implantation were performed 2 weeks apart. Lenses were slowly lowered into the brain and fixed to the skull with dental cement (Metabond, Parkell). Two weeks after lens implantation, mice were head-fixed on a running wheel and a miniaturized micro-endoscope (nVista, Inscopix) was lowered over the implanted lens until GCaMP-expressing fluorescent neurons were in focus. Once GCaMP-expressing neurons were detected, a permanent baseplate was attached to the skull with dental cement. Mice were habituated with weight-matched dummy micro-endoscopes (Inscopix) for at least 1 week before behaviour testing.

Housing conditions for social and sexual experience

All male C57BL/6N mice used in this study were socially and sexually experienced. Mice aged 8–12 weeks were initially co-housed with a female BALB/c mouse for 1 week and were screened for sex-appropriate social behaviours. Mice that showed both mounting towards females and attack towards males during a 30 min resident intruder assay were selected for surgery and subsequent behaviour experiments. From this point forward, these male mice were always co-housed with non-pregnant female BALB/c mice.

Chemogenetic inhibition

Behavioural tests were performed on two consecutive days. The number of mice receiving saline or CNO (Enzo Life Sciences) was counterbalanced across the two days. CNO was dissolved in saline; CNO (7.5 mg kg^{-1}) or saline (control) was intraperitoneally (i.p.) injected 60 min before behavioural tests.

Optogenetic inhibition

Animals were connected to a 470 or 590 nm laser (Changchun New Industries Optoelectronics Tech) via optical patch cords (⌀200 µm, 0.22 numerical aperture; Doric lenses and Thorlabs) and a rotary joint (Doric lenses). The experimenter monitored mouse behaviour via a computer monitor in a room adjacent to the behavioural arena. The laser was triggered manually when animals were engaged in the behaviours of interest. Sham stimulation (laser OFF) was interleaved with light stimulation (laser ON) as an internal control. For optogenetic inhibition of BNSTpr using gtACR2, 10 s of 470 nm continuous photostimulation at 1 mW mm^{-2} at the tissue level was used during social interactions, and 10 min of 470 nm continuous photo stimulation at 1 mW mm^{-2} at the tissue level for urine preference and 'pencil–cup' (meshed barrier) tests. For optogenetic inhibition of BNSTpr/MPOA and BNSTpr/VMHvl terminals using Halorhodopsin, 5 s of 590 nm continuous photostimulation at 3 mW mm^{-2} at the tissue level was used.

Behaviour annotations

Behaviour videos were manually annotated using a custom MATLAB-based behaviour annotation interface[11,43]. A 'baseline' period of 5 min when the animal was alone in its home cage was recorded at the start of every recording session. A total of seven behaviours during the resident intruder assays were annotated: sniff (face, body, genital-directed sniffing) towards male or female intruders, and attack, mount, intromission, 'interact' (periods when the animals were close to each other but sniff, attack and mount/intromission were absent) with male or female intruders. For dangled presentations of male or female intruders, the dangled bouts began at the onset of nostril/whiskers movement when the ano-genital region of the dangled intruder was held next to the resident.

Micro-endoscopic imaging

On the day of imaging, mice were habituated for at least 10 min after installation of the miniscope in their home cage before the start of the behaviour tests. Imaging data were acquired at 30 Hz with 2× spatial downsampling; light-emitting diode power (0.1–0.5) and gain (1–7×) were adjusted depending on the brightness of GCaMP expression as determined by the image histogram according to the user manual. A transistor–transistor logic (TTL) pulse from the Sync port of the data acquisition box (DAQ, Inscopix) was used for synchronous triggering of StreamPix7 (Norpix) for video recording. Imaging sessions typically lasted 1 h (20–25 min of interactions per sex).

ChemoScope imaging

To minimize population activity changes associated with stress from i.p. injections, social experience or fatigue from resident intruder assays in saline or CNO trials, a series of habituation imaging sessions were performed every 2–3 days (three or four sessions in total) before the saline versus CNO trials used for analysis (Extended Data Fig. 5p–s). Mice were injected with 100 μl of saline (or 100 μl of 7.5 mg kg^{-1} CNO for CNO trials) and returned to their home cage for 60 min before imaging.

Micro-endoscopic data extraction

Preprocessing. Miniscope data were acquired using the Inscopix Data Acquisition Software as 2× downsampled .isxd files. Preprocessing and motion correction were performed using Inscopix Data Processing Software. Briefly, raw imaging data were cropped, 2× downsampled, median filtered and motion corrected. A spatial band-pass filter was then applied to remove out-of-focus background. Filtered imaging data were temporally downsampled to 10 Hz and exported as a .tiff image stack.

Calcium data extraction. After preprocessing, calcium traces were extracted and deconvolved using the CNMF-E large data pipeline[32] with the following parameters: patch_dims = [42, 42], gSig = 3, gSiz = 13, ring_radius = 19, min_corr = 0.8, min_pnr = 8, deconvolution: foopsi with the ar1 model[44]. The spatial and temporal components of every extracted unit were carefully inspected manually (SNR, PNR, size, motion artefacts, decay kinetics and so on) and outliers (obvious deviations from the normal distribution) were discarded. The extracted traces were then *z*-scored before analysis.

Choice probability

Choice probability is a metric that estimates how well either of two different behaviours can be predicted/distinguished, based on the activity of any given neuron during these two behaviours[45]. CP of single neurons was computed using previously described methods[9,19]. To compute the CP of a single neuron for any behaviour pair, 1 s binned neuronal responses occurring during each of the two behaviours were used to generate a receiver operating characteristic curve. CP is defined as the area under the curve bounded between 0 and 1. A CP of 0.5 indicates that the activity of the neuron cannot distinguish between the two alternative behaviours. We defined a neuron as being capable of distinguishing between two behaviours (for example, interacting with male versus female) if the CP of that neuron was >0.65 or <0.35 and was >2 σ or <−2 σ of the CP computed using shuffled data (repeated 100 times). For instance, if the CP of a particular neuron for females was 0.8 and the shuffled CP was 0.5 ± 0.1 (s.d.), that neuron would be considered as female-preferring; if another neuron had a CP of 0.1 and a shuffled CP of 0.5 ± 0.15 (s.d.), that neuron would be considered as male-preferring.

Decoding intruder sex

We constructed either frame-wise (using 1 s binned behaviour and calcium activity frames; Fig. 3l) or time-evolving (as a function of time at 10 Hz; Figs. 2i and 3m) linear SVM decoders (as described previously[9]) to distinguish intruder sex using 50 randomly selected neurons from each animal in BNST (*n* = 15 animals), VMHvl (*n* = 7) and MPOA (*n* = 7). Accuracy was evaluated using a stratified fivefold cross-validator. Decoding was repeated 100 times, with decoder performance reported as the mean accuracy per imaged animal. For significance testing, the mean accuracy of the decoder trained on shuffled data (repeated 500 times per imaged animal) was computed to compare against the decoder accuracy trained on actual data.

Determination of explained variance in BNSTpr population activity

We calculated the variance in population activity explained by intruder sex and behaviours (Fig. 2o) using linear regression as described previously[9]. To evaluate the encoding of intruder sex and behaviours by BNSTpr^{Esr1} neurons, we regressed the activity of single neurons against the sex of the intruder (a pair of binary vectors) and against seven annotated behaviours (seven binary vectors). The fraction of variance explained is calculated as the ratio of the cross-validated R^2 (coefficient of determination) of the fit against the sex of the intruder and the cross-validated R^2 of the fit against seven different behaviours. To determine the fraction of variance explained by behaviours, we regressed the residual activity (from the fit against intruder sex) against male- or female-directed behaviours and reported the fraction of the residual variance explained, as cross-validated R^2 of the fit.

Pearson's correlation

Pearson's correlation (Fig. 3j) was reported as the mean pair-wise Pearson's correlation coefficient per imaged animal computed using the average population responses (all trials during one recording session) to dangled male intruders and the 1 s binned population responses to dangled male intruders (same sex) or dangled female intruders (opposite sex).

Mahalanobis distance ratio

Mahalanobis distance ratio (Fig. 3k) was expressed as the ratio between the Mahalanobis distance (described previously[19]) of the population vector responding to dangled female intruders (opposite sex) and the Mahalanobis distance of the population vector responding to dangled male intruders (same sex).

Supervised UMAP embedding of single-unit responses to male and female stimuli

The first 50 PCs of 1 s binned single-unit responses to male and female stimuli from MPOA and VMHvl, along with categorical labels indicating the origin of each unit (MPOA pre-CNO, MPOA CNO, VMHvl pre-CNO, VMHvl CNO), were used to initialize embedding (Fig. 3q). The Python implementation of UMAP[46] (umap-learn) was used along with the following parameters: n_neighbors = 15, min_dist = 0.4, metric = euclidean.

Statistical analysis

Data were processed and analysed using Python, MATLAB and GraphPad (GraphPad PRISM v.9). All data were analysed using two-tailed, non-parametric tests except for urine preference and pencil–cup (meshed barrier) tests (Extended Data Fig. 1r,w), and the fraction of variance explained by intruder sex or female-directed behaviour (Fig. 5g) when two-way ANOVA with Bonferroni correction was used. Wilcoxon signed-rank test (paired, non-parametric Mann–Whitney *U*-test) was used for binary paired samples. Friedman's test with Dunn's correction was used for non-binary paired samples (Fig. 5d,f), and Kolmogorov–Smirnov test for non-paired samples. n.s., $P > 0.05$, $^{*}P < 0.05$, $^{**}P < 0.01$, $^{***}P < 0.001$, $^{****}P < 0.0001$.

Reporting summary

Further information on research design is available in the Nature Research Reporting Summary linked to this paper.

Data availability

The data on which this study is based are available on reasonable request.

Code availability

The custom MATLAB and Python codes used to analyse the data in this study are available on request.

42. Daigle, T. L. et al. A suite of transgenic driver and reporter mouse lines with enhanced brain-cell-type targeting and functionality. *Cell* **174**, 465–480 (2018).
43. Segalin, C. et al. The Mouse Action Recognition System (MARS) software pipeline for automated analysis of social behaviors in mice. *eLife* **10**, e63720 (2021).
44. Friedrich, J., Zhou, P. & Paninski, L. Fast online deconvolution of calcium imaging data. *PLoS Comput. Biol.* **13**, e1005423 (2017).
45. Shadlen, M., Britten, K., Newsome, W. & Movshon, J. A computational analysis of the relationship between neuronal and behavioral responses to visual motion. *J. Neurosci.* **16**, 1486–1510 (1996).
46. McInnes, L., Healy, J. & Melville, J. UMAP: Uniform manifold approximation and projection for dimension reduction. Preprint at https://doi.org/10.48550/arXiv.1802.03426 (2020).

Acknowledgements We thank A. Kennedy and A. Nair for advice on miniscope data analysis; M. Hui and C. Kim for assistance with animal surgery and behaviour experiments; M. Zelikowsky for advice on statistical analysis; W. Hong for pilot experiments performed on BNSTpr; X. Da, J. Chang and X. Wang for histology; Y. Huang for genotyping; Caltech OLAR staff for animal care; J. Costanza for mouse colony management; M. Schnitzer, A. Vinograd and B. Weissbourd for constructive comments on the manuscript; C. Chiu for laboratory management; G. Mancuso for administrative assistance; and members of the Anderson laboratory for helpful comments on this project. This paper was supported by NIH grant nos. MH070053, MH112593 and NS123916 and by the Simons Collaboration on the Global Brain. D.J.A. is an investigator of the Howard Hughes Medical Institute.

Author contributions B.Y. performed experiments, analysed data and prepared figures. T.K. performed retrograde tracing experiments. B.Y. and D.J.A. designed the study and wrote the paper.

Competing interests The authors declare no competing interests.

Additional information

Supplementary information The online version contains supplementary material available at https://doi.org/10.1038/s41586-022-05057-6.

Correspondence and requests for materials should be addressed to David J. Anderson.

Peer review information *Nature* thanks the anonymous reviewers for their contribution to the peer review of this work. Peer reviewer reports are available.

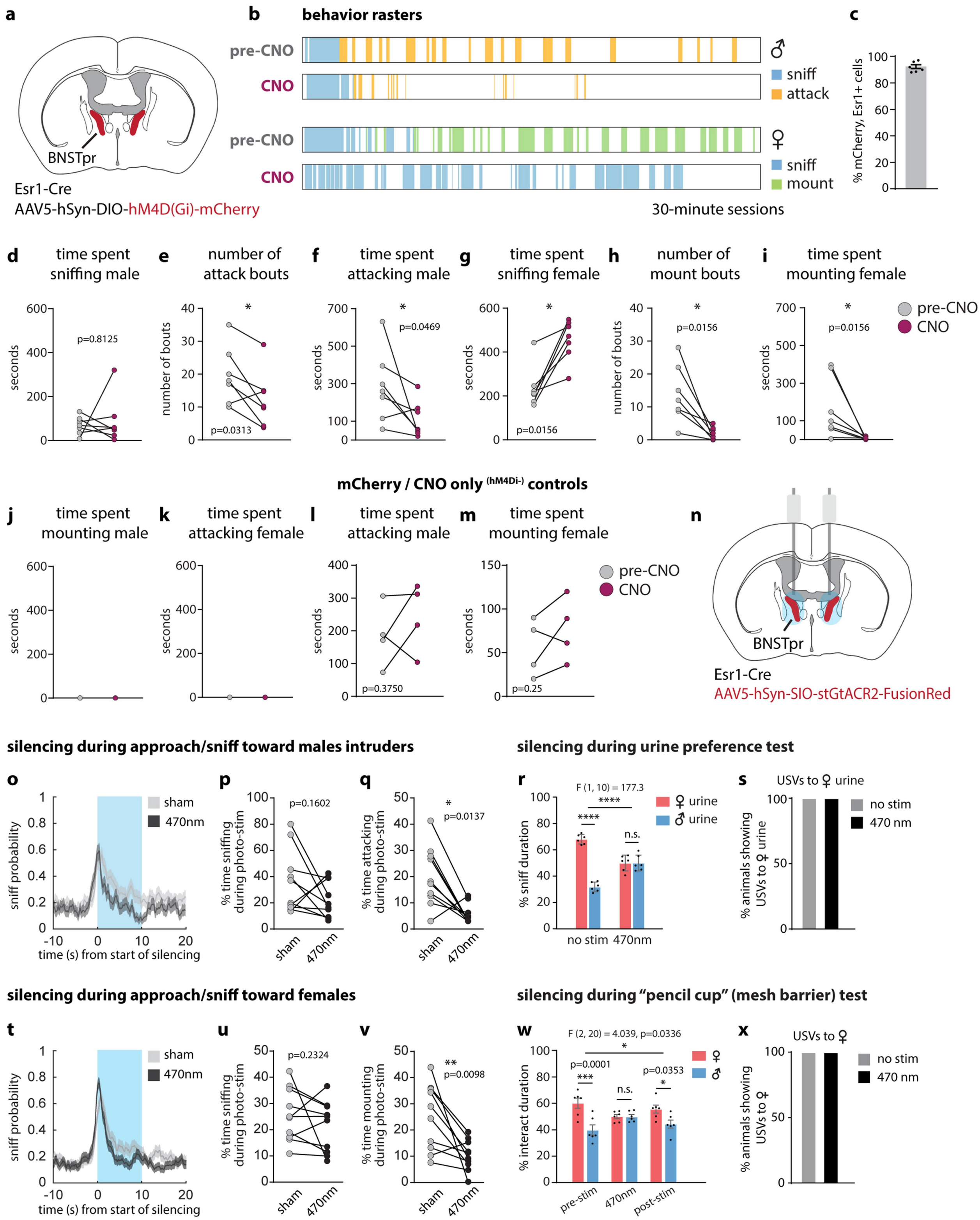

Extended Data Fig. 1 | See next page for caption.

Extended Data Fig. 1 | Chemogenetic and optogenetic silencing of BNSTpr^{Esr1} neurons disrupts aggression and mating. **a**, Illustration of hM4d (Gi)-mediated silencing in bilateral BNSTpr^{Esr1} neurons. **b**, Example behavior raster plot from 1 animal across 4 recording sessions. **c**, Percent of BNSTpr^{Esr1} neurons that express mCherry. Values are plotted as mean ± SEM, n = 6 mice. **d**–**m**, Measurements performed before (pre-CNO: saline injection, gray points) vs. after (CNO injection, maroon points) chemogenetic silencing of BNSTpr, of time spent sniffing male intruders (**d**), number of attack bouts toward male intruders (**e**), time spent attacking male intruders (**f**), time spent sniffing female intruders (**g**), number of mount bouts toward female intruders (**h**), time spent mounting female intruders (**i**), time spent mounting male intruders (**j**), time spent attacking female (**k**), and time spent attacking male (**l**), time spent mounting female (**m**) in mCherry/CNO only controls (**l**, **m**) per 30-minute session. 100µl containing either saline (pre-CNO) or 7.5mg/kg CNO was given i.p. 60 min prior to start of behavior tests. **n**, Illustration of bilateral optogenetic silencing in BNSTpr. **o**, **t**, Mean probability of sniff behavior occurring relative to onset of optogenetic silencing. **p**, **u**, Duration of sniffing toward male (**p**) or female (**u**) intruders. **q**, **v**, Duration of attack (**q**) toward male intruders or mount (**v**) toward female intruders as a percentage of the duration of optogenetic silencing. "Sham" controls were the same animals during a 10s "sham stimulation," i.e., without light. **r**, **w**, Percent of time spent interacting with male or female urine (r), or male or female conspecifics separated by a meshed barrier (**w**) before and during (**r**) or before, during and after (**w**) optogenetic silencing of BNSTpr. Optogenetic silencing conditions: 470nm @ ~1 mW/mm^2 for 10 s (**o**, **p**, **q**, **t**, **u**, **v**). 470nm @ ~1 mW/mm^2 for 10 min (**r**, **s**, **w**, **x**) Statistics: For Chemogenetic inhibition, two-sided Wilcoxon signed-rank test (**d**–**m**). Values are plotted as total time or total bouts per 30-minute session per animal. n = 7 mice (**d**–**k**), n = 4 mice (**l**, **m**). For Optogenetic inhibition during interactions with male or female conspecifics (**o**, **p**, **q**, **t**, **u**, **v**), two-sided Kolmogorov-Smirnov test (**o**, **t**), two-sided Wilcoxon signed-rank test (**p**, **q**, **u**, **v**). Male-male trials (**o**, **p**, **q**), n = 131 stim and 125 sham trials pooled from 10 mice. Male-female trials mice (**t**, **u**, **v**), n = 181 stim and 170 sham trials pooled from 10 mice. For Optogenetic inhibition during urine preference (**r**) and "pencil cup" (mesh barrier) (**w**) tests, two-way ANOVA with Bonferroni correction, n = 6 mice. Values are plotted as mean ± SEM. ****$p < 0.0001$; ***$p < 0.001$; **$p < 0.01$; *$p < 0.05$. The mouse brain images in this figure (**a**, **n**) have been reproduced from ref. [41].

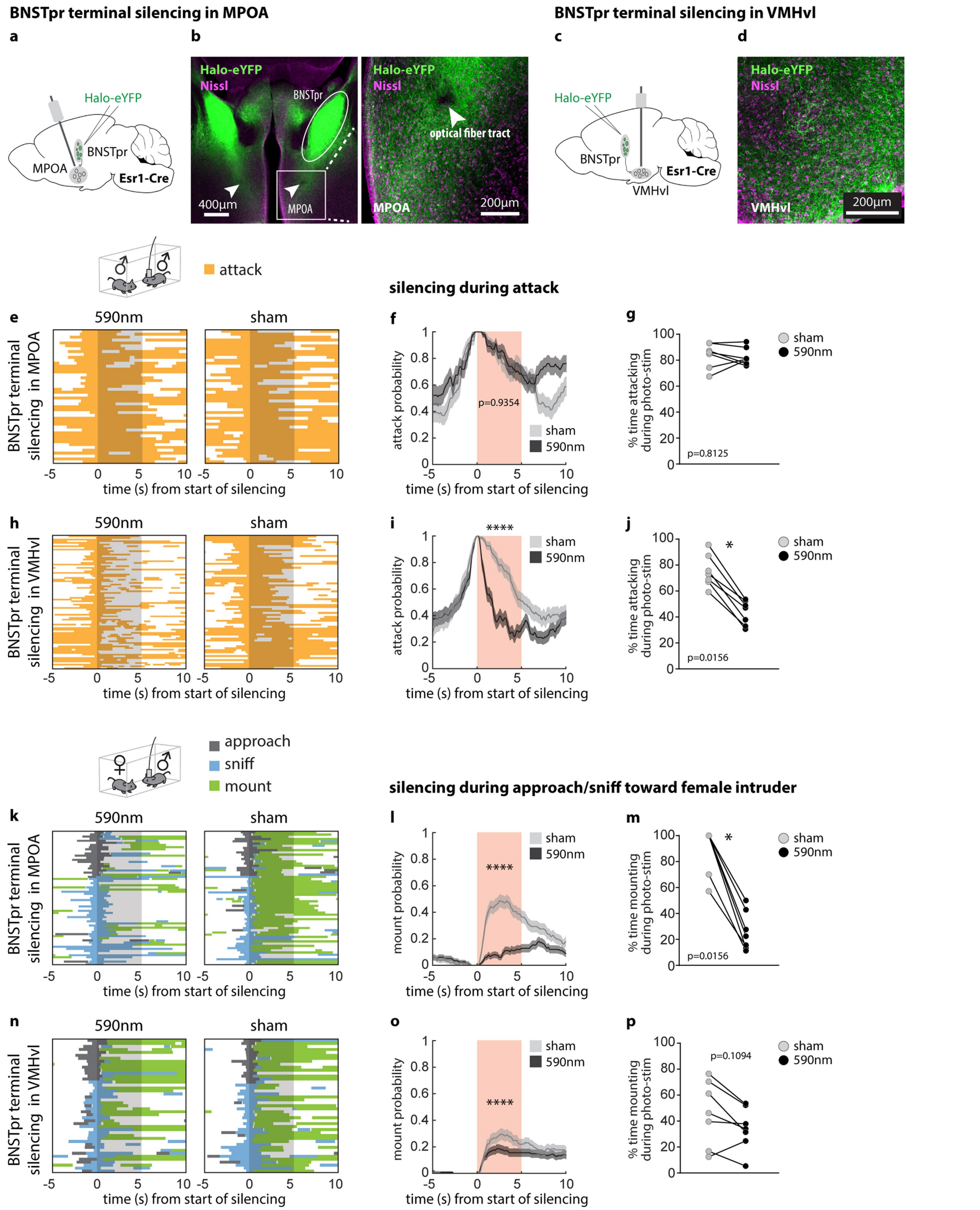

Extended Data Fig. 2 | Optogenetic silencing of BNSTpr^{Esr1} terminals in MPOA or VMHvl during male-male/ male-female interactions. **a**, **c**, Diagram illustrating BNST terminal silencing in MPOA (**a**) or VMHvl (**c**). **b**, **d**, Representative images showing cre-dependent Halo-EYFP cell body expression in BNSTpr and axonal expression in MPOA (**b**) and VMHvl (**d**). Similar expression patterns were observed in all 14 animals tested (**b**, **d**). **e**, **h**, **k**, **n**, Raster plots showing distribution of social behaviors relative to optogenetic silencing of BNSTpr terminal in MPOA (**e**, **k**) or VMHvl (**h**, **n**). **f**, **i**, **l**, **o**, Average probability of behavior occurring relative to onset of optogenetic silencing. **g**, **j**, **m**, **p**, Duration of attack (**g**, **j**) or mount (**m**, **p**) as a percentage of the 5-second optogenetic silencing. Statistics: two-sided Kolmogorov-Smirnov test (**f**, **i**, **l**, **o**), values are plotted as mean ± SEM. Two-sided Wilcoxon signed-rank test (**g**, **j**, **m**, **p**). ****$p < 0.0001$; ***$p < 0.001$; **$p < 0.01$; *$p < 0.05$. n = 7 mice for each silenced region. The mouse brain images in this figure (**a**, **c**) have been reproduced from ref. [41].

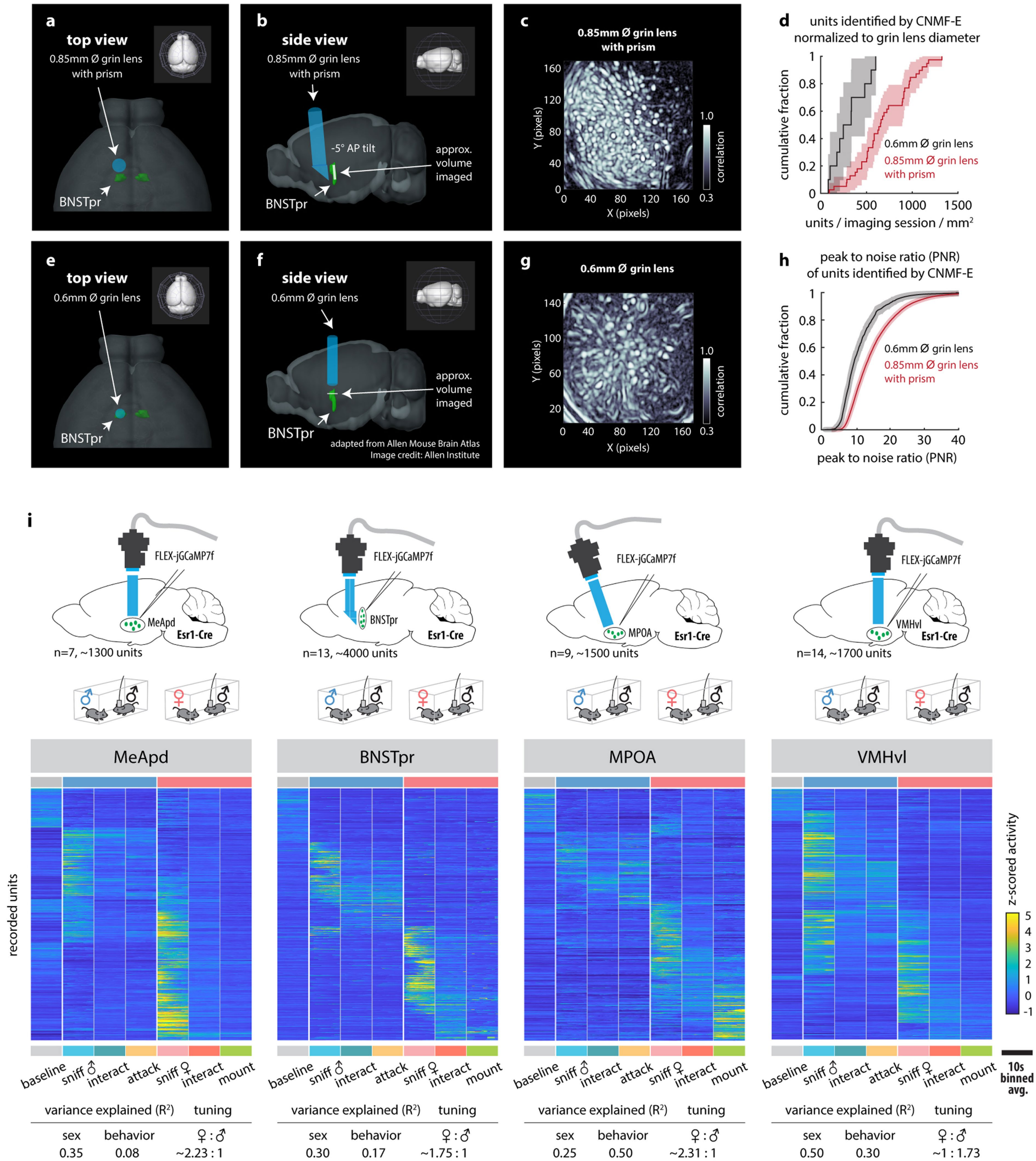

Extended Data Fig. 3 | Performance of 0.85 mm Ø prism coupled GRIN lens compared to 0.6 mm Ø GRIN lens for imaging BNSTpr. a, **b**, **d**, **e**, Illustrations showing GRIN lens placement in BNSTpr from top (**a**, **d**) and side (**b**, **e**) views. **a**–**c**, Illustrations or data from animals implanted with prism lenses. **d**–**f**, Data from animals implanted with conventional cylindrical GRIN lenses. **c**, **f**, Mean pixel correlation during 1 example imaging session. **g**, Cumulative fraction of number of units captured per imaging session normalized to the diameter of the GRIN lens. **h**, Cumulative fraction of the peak to noise ratio (PNR) of all units imaged using either a 0.6mm grin lens or a 0.85mm prism-coupled grin lens. **i**, Raster plots of MeApd, BNSTpr, MPOA and VMHvl $Esr1^{+}$ neuronal activity during male-male or male-female unrestrained social interactions. For comparative purposes, all frames containing each behavior scored (indicated below plot) during a 30 min social interaction were concatenated and binned into 10s intervals; Averaged z-scored responses of each unit across all bins are shown. Tables below show the average variance (R^2) in population activity that can be explained by intruder sex or by male and female-directed consummatory behavior and the ratio of female-preferring to male-preferring neurons in each imaged region. The mouse brain image in this figure (**i**) has been reproduced from ref. [41].

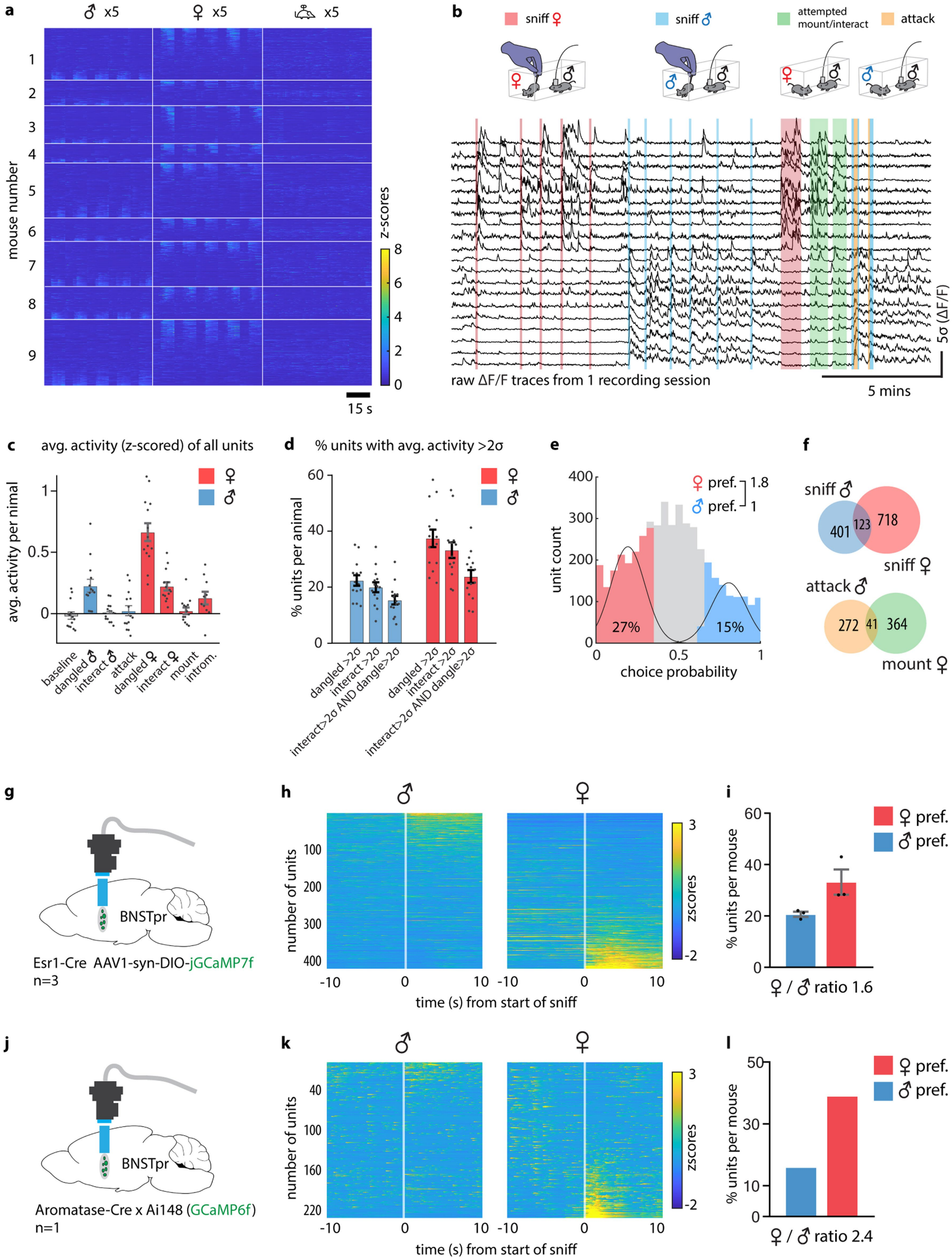

Extended Data Fig. 4 | Miniscope imaging analysis of BNSTpr neurons. **a**, Example raster plot of population responses to 5 repeated presentations of dangled male, female or toy intruders from a cohort of 9 individual animals (cohort 1, n = 6, cohort 2, n = 9). **b**, continuously recorded raw ΔF/F traces of 20 example neurons from 1 recording session. **c**, Average z-scored responses of BNSTpr neurons per animal (n = 15 mice) during 8 annotated behaviors/conditions. **d**, Percent of units per animal (n = 15 mice) whose average response is >2σ baseline measured prior to intruder introduction. **e**, Histograms of male-/female-preferring units determined by choice probability from single-unit responses to dangled intruders. **f**, Venn diagram of units that are male- or female- sniff preferring (top), or attack- or mount- preferring (bottom) (determined by choice probability) during free interactions with, or sniffing of dangled, male or female intruders. **g–l**, Comparison of BNSTpr^{Esr1} (**g**, **h**, **i**) and BNSTpr^{AB} (**j**, **k**, **l**) population responses to dangled presentation of male or female intruders. **g**, **j**, Illustration of BNSTpr^{Esr1} (**g**) and BNSTpr^{AB} (**j**) miniscope imaging using a conventional 0.6mm GRIN lens. **h**, **k**, Average z-scores of single-unit responses relative to the start of sniff during 5 repeated dangling presentations of male or female intruders. **i**, **l**, percent of male vs female preferring units in BNSTpr. n = 15 mice. The mouse brain images in this figure (**g**, **j**) have been reproduced from ref. [41].

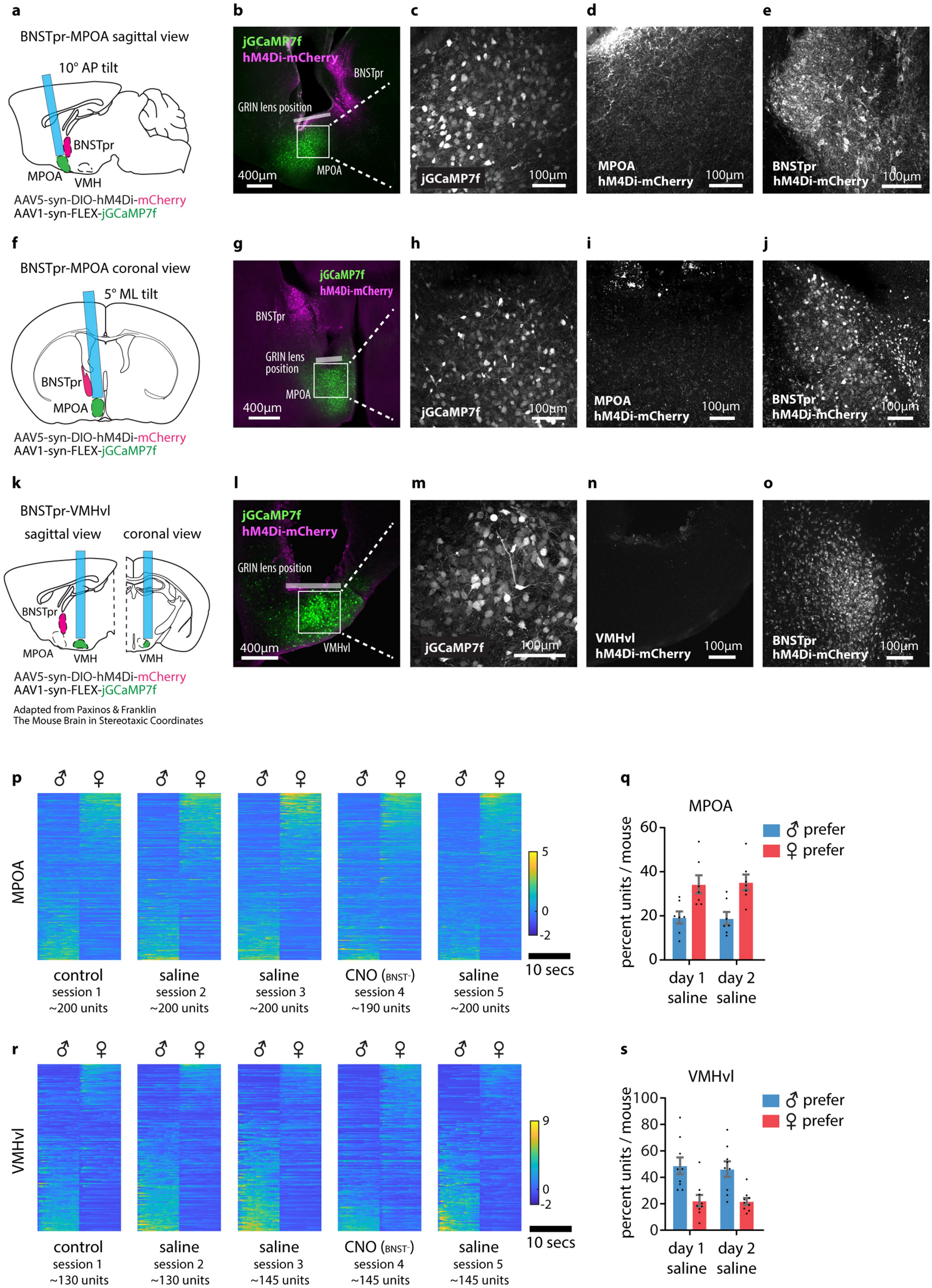

Extended Data Fig. 5 | See next page for caption.

Extended Data Fig. 5 | ChemoScope imaging of MPOA and VMHvl across multiple days. a, **f**, **k**, Diagram showing the position of 0.6mm GRIN lens in relation to MPOA, BNSTpr and VMHvl. **b**–**e**, Sagittal histology sections showing the expression of jGCaMP7f in MPOA (**b**, **c**), hM4Di-mCherry in BNSTpr (**b**, **e**), and lack of cell body expression of hM4Di-mCherry in MPOA (**d**). **g**–**j**, Coronal histology sections showing the expression of jGCaMP7f in MPOA (**g**, **h**), hM4Di-mCherry in BNSTpr (**g**, **j**), and lack of cell body expression of hM4Di-mCherry in MPOA (**i**). **l**–**o**, Coronal histology sections showing the expression of jGCaMP7f VMHvl (**l**, **m**), hM4Di-mCherry in BNSTpr (**o**), and lack of cell body expression of hM4Di-mCherry in VMHvl (**n**). Similar expression patterns were observed in 14 mice tested (7 mice for each imaged region). **p**, **r**, example raster plots of average single-unit responses to 5 trials of dangled male or female intruders in MPOA (**p**) and VMHvl (**r**) across multiple imaging sessions (sessions are 2-3 days apart). Units are sorted based on their eigenvalues in the first principal component of the population activity vector. **q**, **s**, percent of units that are male or female preferring across 2 days of imaging in MPOA (**q**) and VMHvl (**s**), in saline-injected animals. n = 7 mice from each imaged region.

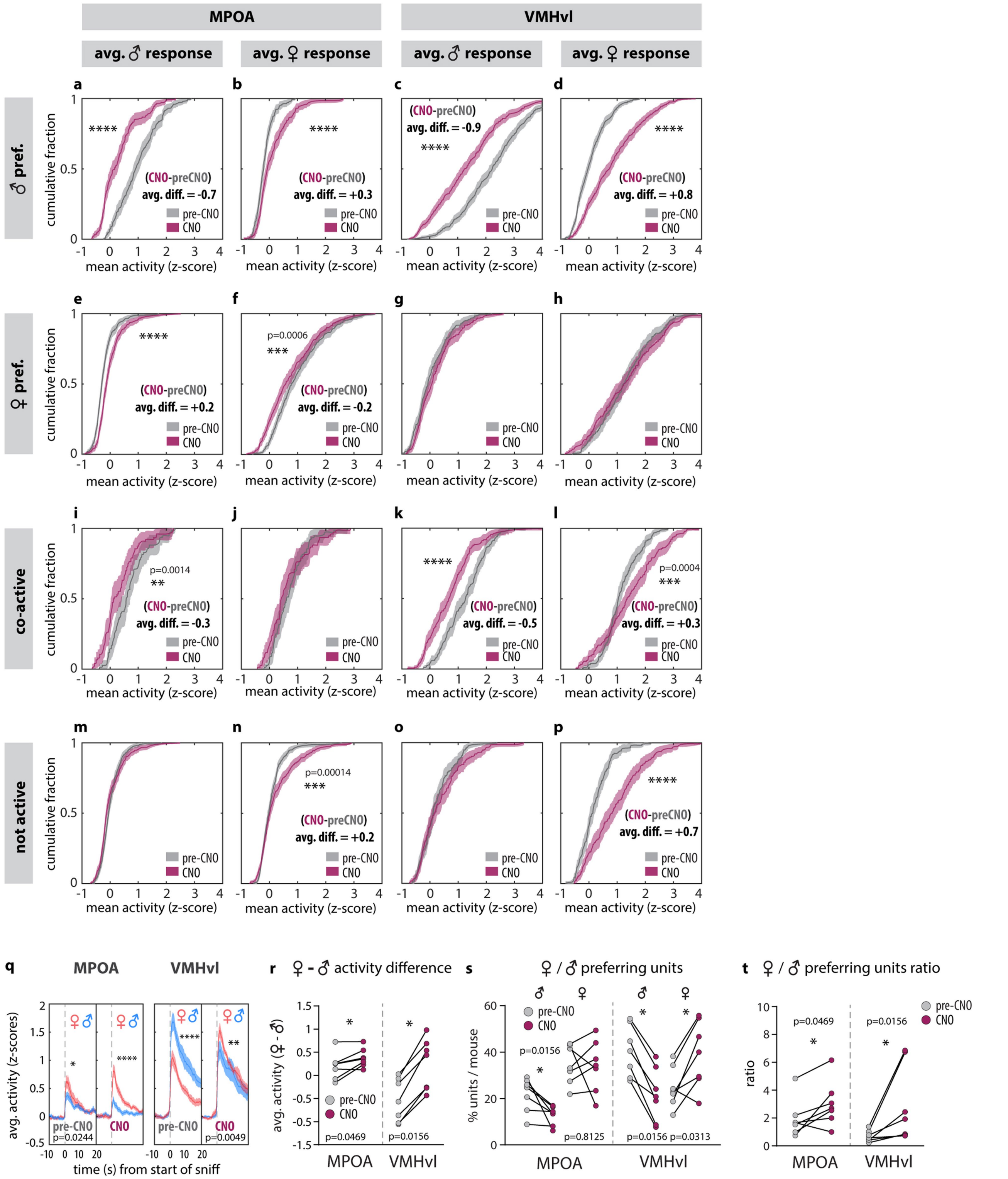

Extended Data Fig. 6 | ChemoScope imaging of MPOA and VMHvl. **a**–**p**, Cumulative fractions showing average single unit responses to dangled male and female intruders from initially (i.e., in saline-injected animals) male preferring (**a**–**d**), female preferring (**e**–**h**), co-active (**i**–**l**) and not active (**m**–**p**) units in MPOA (**a**, **b**, **e**, **f**, **i**, **j**, **m**, **n**) and VMHvl (**c**, **d**, **g**, **h**, **k**, **l**, **o**, **p**). **q**, average responses to dangled male or female intruders in MPOA (left panel) and VMHvl (right panel). **r**–**t**, mean response difference between dangled female and male intruders (**r**), percentage of male vs female preferring units (**s**) and the ratio of female- to male-preferring units (**t**) before and after the application of CNO, in MPOA or VMHvl. Statistics: two-sided Kolmogorov-Smirnov test (**a**–**q**), values are plotted as mean ± SEM. Two-sided Wilcoxon signed-rank test (**r**–**t**). ****$p < 0.0001$; ***$p < 0.001$; **$p < 0.01$; *$p < 0.05$. n = 7 mice from each imaged region.

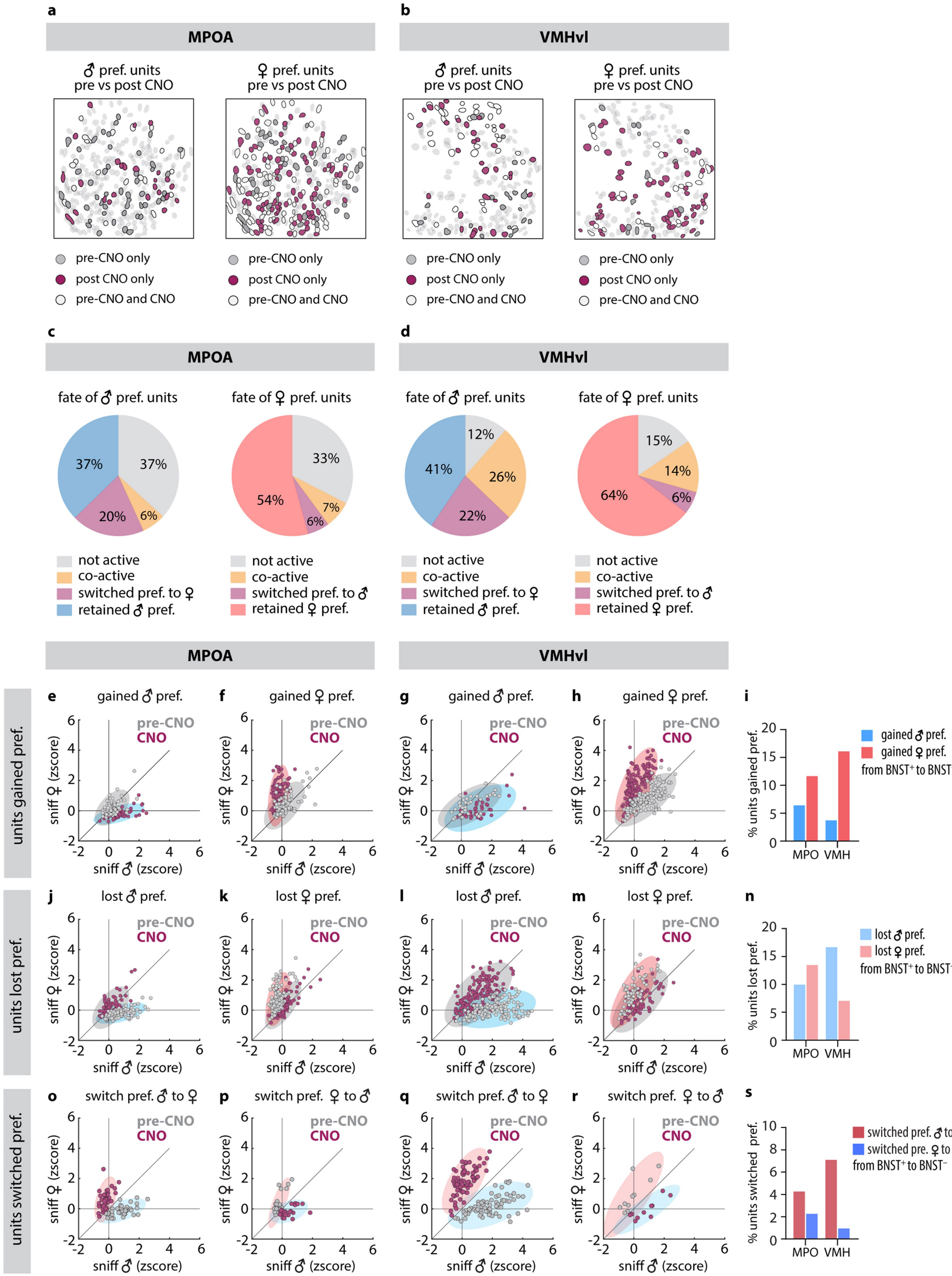

Extended Data Fig. 7 | Tracking changes to MPOA and VMHvl single-unit responses before and after silencing BNSTpr. a, **b**, Spatial maps showing distribution of male- or female preferring units before (gray) and after (maroon) chemogenetic silencing of BNSTpr in MPOA(**a**) or VMHvl (b). **c**, **d**, response profiles of initially (i.e., in saline-injected animals/pre-CNO) male- or female preferring units after BNSTpr silencing, in MPOA (**c**) and VMHvl (**d**). (**e**–**s**) 2d scatter plots and bar plots showing average single-unit responses to dangled male and female intruders from tracked units in MPOA and VMHvl, sorted as indicated.

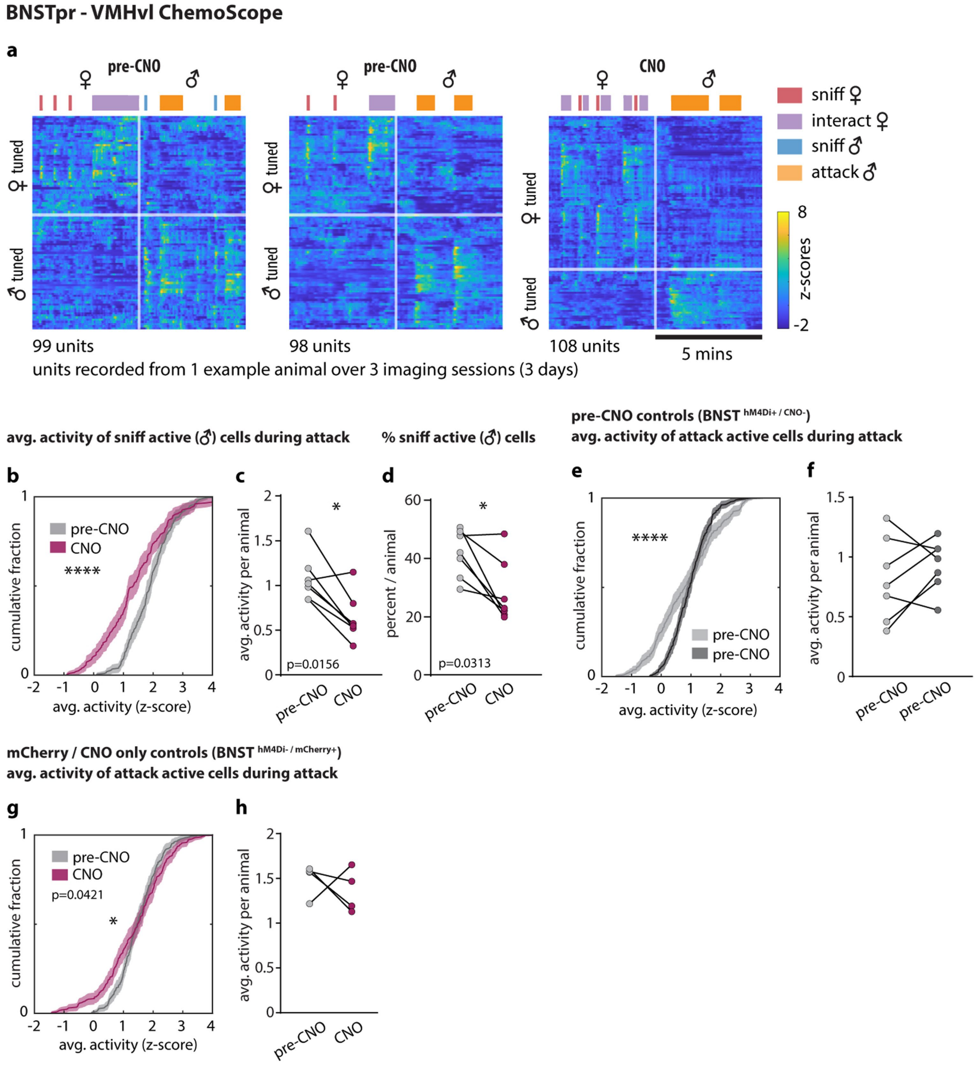

Extended Data Fig. 8 | Effect of BNSTpr silencing on VMHvl behavior representations and female / male preference. **a**, Raster plot of all recorded units from 1 example animal over 3 imaging sessions. Units are sorted separately for each recorded session based on their responses during male and female interactions. **b**, **c**, **e**–**h**, Cumulative fractions (**b**, **e**, **g**) and bar graphs (**c**, **f**, **h**) of VMHvl single-unit responses to initially (i.e., in saline-injected animals/pre-CNO) sniff active (**b**, **c**) or attack active (**e**–**h**) cells during attack before CNO (i.e., saline-injected/pre-CNO) (**e**, **f**), or before and after CNO (**b**, **c**, **g**, **h**). **g**, **h**, mCherry/CNO only controls. **d**, percent sniff active cells in VMHvl before (i.e., saline-injected/pre-CNO) and after CNO. Statistics: two-sided Kolmogorov-Smirnov test (**b**, **e**, **g**), values are plotted as mean ± SEM, two-sided Wilcoxon signed-rank test (**c**, **d**, **f**, **h**). ****$p < 0.0001$; ***$p < 0.001$; **$p < 0.01$; *$p < 0.05$. n = 7 mice.

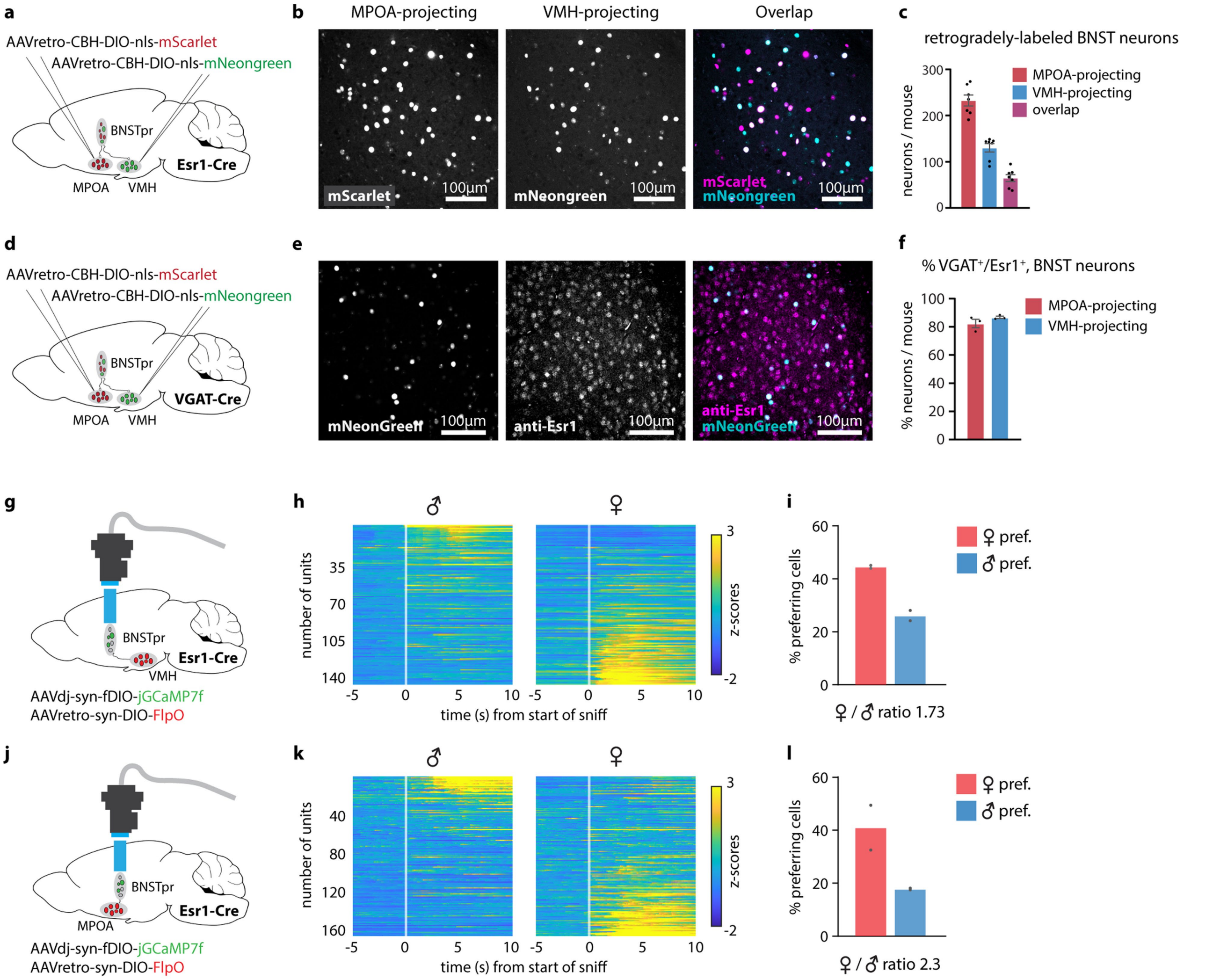

Extended Data Fig. 9 | Retrograde tracing and imaging of BNSTpr projection neurons. **a**, **d**, Diagram showing retrograde tracing of BNSTpr projection neurons. **b**, **e**, Example images showing MPOA or VMHvl projecting neurons expressing mScarlet or mNeongreen. **c**, Average number of back-labeled BNSTpr neurons per animal. n = 7 mice. **f**, Percent of VGAT^{+} projection neurons that are Esr1^{+}. n = 3 mice per injected region. Values are plotted as mean ± SEM (**c**, **f**). **g**, **j**, Diagram showing miniscope imaging of VMHvl-projecting (n = 2 mice) or MPOA-projecting (n = 2 mice) BNSTpr neurons. **h**, **k**, Average z-scores of single-unit responses relative to the start of sniff during 5 repeated dangling presentations of male or female intruders (n = 2 mice per injected region). **i**, **l**, Percent of male- or female-preferring units (n = 2 mice per injected region). The mouse brain images in this figure (**a**, **b**, **g**, **j**) have been reproduced with permission from ref. [41].

nature portfolio

Corresponding author(s): David J. Anderson

Last updated by author(s): Jun 5, 2022

Reporting Summary

Nature Portfolio wishes to improve the reproducibility of the work that we publish. This form provides structure for consistency and transparency in reporting. For further information on Nature Portfolio policies, see our Editorial Policies and the Editorial Policy Checklist.

Statistics

For all statistical analyses, confirm that the following items are present in the figure legend, table legend, main text, or Methods section.

n/a	Confirmed	
☐	☒	The exact sample size (*n*) for each experimental group/condition, given as a discrete number and unit of measurement
☐	☒	A statement on whether measurements were taken from distinct samples or whether the same sample was measured repeatedly
☐	☒	The statistical test(s) used AND whether they are one- or two-sided *Only common tests should be described solely by name; describe more complex techniques in the Methods section.*
☐	☒	A description of all covariates tested
☐	☒	A description of any assumptions or corrections, such as tests of normality and adjustment for multiple comparisons
☐	☒	A full description of the statistical parameters including central tendency (e.g. means) or other basic estimates (e.g. regression coefficient) AND variation (e.g. standard deviation) or associated estimates of uncertainty (e.g. confidence intervals)
☐	☒	For null hypothesis testing, the test statistic (e.g. *F*, *t*, *r*) with confidence intervals, effect sizes, degrees of freedom and *P* value noted *Give P values as exact values whenever suitable.*
☒	☐	For Bayesian analysis, information on the choice of priors and Markov chain Monte Carlo settings
☒	☐	For hierarchical and complex designs, identification of the appropriate level for tests and full reporting of outcomes
☒	☐	Estimates of effect sizes (e.g. Cohen's *d*, Pearson's *r*), indicating how they were calculated

Our web collection on statistics for biologists contains articles on many of the points above.

Software and code

Policy information about availability of computer code

Data collection	StreamPix 7 for Behavior video acquisition, Inscopix data acquisition software for Microendoscope recording
Data analysis	Python3.6 for analysis of calcium imaging data, MATLAB 2019b for Behavior annotations and analysis of calcium imaging data, GraphPad Prism 8 and MATLAB 2018b for statistical analyses, Adobe Illustrator Ver.25 for assembling figures

For manuscripts utilizing custom algorithms or software that are central to the research but not yet described in published literature, software must be made available to editors and reviewers. We strongly encourage code deposition in a community repository (e.g. GitHub). See the Nature Portfolio guidelines for submitting code & software for further information.

Data

Policy information about availability of data

All manuscripts must include a data availability statement. This statement should provide the following information, where applicable:
- Accession codes, unique identifiers, or web links for publicly available datasets
- A description of any restrictions on data availability
- For clinical datasets or third party data, please ensure that the statement adheres to our policy

The data on which this study is based are available upon reasonable request.

Human research participants

Policy information about studies involving human research participants and Sex and Gender in Research.

Reporting on sex and gender	*Use the terms sex (biological attribute) and gender (shaped by social and cultural circumstances) carefully in order to avoid confusing both terms. Indicate if findings apply to only one sex or gender; describe whether sex and gender were considered in study design whether sex and/or gender was determined based on self-reporting or assigned and methods used. Provide in the source data disaggregated sex and gender data where this information has been collected, and consent has been obtained for sharing of individual-level data; provide overall numbers in this Reporting Summary. Please state if this information has not been collected. Report sex- and gender-based analyses where performed, justify reasons for lack of sex- and gender-based analysis.*
Population characteristics	*Describe the covariate-relevant population characteristics of the human research participants (e.g. age, genotypic information, past and current diagnosis and treatment categories). If you filled out the behavioural & social sciences study design questions and have nothing to add here, write "See above."*
Recruitment	*Describe how participants were recruited. Outline any potential self-selection bias or other biases that may be present and how these are likely to impact results.*
Ethics oversight	*Identify the organization(s) that approved the study protocol.*

Note that full information on the approval of the study protocol must also be provided in the manuscript.

Field-specific reporting

Please select the one below that is the best fit for your research. If you are not sure, read the appropriate sections before making your selection.

☒ Life sciences ☐ Behavioural & social sciences ☐ Ecological, evolutionary & environmental sciences

For a reference copy of the document with all sections, see nature.com/documents/nr-reporting-summary-flat.pdf

Life sciences study design

All studies must disclose on these points even when the disclosure is negative.

Sample size	No statistics were used to determine sample sizes. Sample sizes were determined based on our previous experiments to sufficiently detect meaningful biological differences with good reproducibility (Lee et al., 2014, Remedios and Kennedy et al., 2017 and Karigo et al., 2020 cited in the manuscript).
Data exclusions	Animals in which the virus injection and/or implantation missed the target brain region were excluded from analysis.
Replication	All the experiments were repeated at least two times with separate cohort of animals and the reproducibility was confirmed.
Randomization	For imaging experiments, animals were randomly chosen from Esr1-Cre transgenic cohort.
Blinding	The experimenter was blind to experimental or control groups during data collection and analyses.

Reporting for specific materials, systems and methods

We require information from authors about some types of materials, experimental systems and methods used in many studies. Here, indicate whether each material, system or method listed is relevant to your study. If you are not sure if a list item applies to your research, read the appropriate section before selecting a response.

Materials & experimental systems

n/a	Involved in the study
☒	☐ Antibodies
☒	☐ Eukaryotic cell lines
☒	☐ Palaeontology and archaeology
☐	☒ Animals and other organisms
☒	☐ Clinical data
☒	☐ Dual use research of concern

Methods

n/a	Involved in the study
☒	☐ ChIP-seq
☒	☐ Flow cytometry
☒	☐ MRI-based neuroimaging

Animals and other research organisms

Policy information about studies involving animals; ARRIVE guidelines recommended for reporting animal research, and Sex and Gender in Research

Laboratory animals	Experiments were performed on male and female C57BL6N and BALB/c mice, between 8 and 24 weeks of age. All mice were housed in ventilated micro-isolator cages in a temperature-controlled environment (median temperature 23 °C, humidity 60%), under a reversed 11 h dark– 13h light cycle, with ad libitum access to food and water. Mouse cages were changed weekly.
Wild animals	The study did not involve wild animals.
Reporting on sex	Findings from this study only applies to males and not females.
Field-collected samples	The study did not involve field-collected samples.
Ethics oversight	All experimental procedures involving the use of live animals or their tissues were carried out in accordance with the NIH guidelines and approved by the Institutional Animal Care and Use Committee and the Institutional Biosafety Committee at the California Institute of Technology.

Note that full information on the approval of the study protocol must also be provided in the manuscript.